SECTION 2

THERMAL AND FAST REACTOR MATERIALS

https://doi.org/10.46813/2022-140-066

UDC 621.039.1(075.8)

A REVIEW: FERRITIC-MARTENSITIC STEELS – TREATMENT, STRUCTURE AND MECHANICAL PROPERTIES

H.Yu. Rostova, G.D. Tolstolutska
National Science Center "Kharkov Institute of Physics and Technology", Kharkiv, Ukraine
E-mail: veg-annie@ukr.net

The constantly growing consumption of electricity requires the development and implementation of more powerful and energy-intensive systems of the new generation. Fusion and fission reactors of the 4th generation (Gen-IV) will make it possible to cover the growing demand for electricity. Since Gen-IV reactors will operate at higher temperatures and radiation doses, the problem of selecting scientifically based structural materials arises, since conventional reactor materials are not suitable for use in such severe operating conditions. Among the structural materials under consideration for future generations of reactors, special attention is paid to 9…12% Cr ferritic-martensitic steels due to their higher radiation tolerance and excellent mechanical properties compared to traditionally used austenitic steels. This review presents the main ferritic-martensitic steels that will be used as structural materials, their structure, mechanical properties and various thermal and thermomechanical treatments applied to them.

INTRODUCTION

Most of the industrial nuclear reactors operating in the world are of the second generation category. Generation III reactors have just begun to be used, and Generation III+ reactors are in the commercialization stage. Although the safety and reliability of these reactors are very high, it is widely recognized that nuclear power plays a critical role in meeting the world's ever-increasing energy needs. In 2000, the Gen-IV initiative was created – an international alliance between ten countries and the European Union, and the number of participating countries is growing [1]. This initiative calls for the creation of new nuclear power systems that will significantly improve safety and reliability, sustainability, reactor useful life (60 years or more) and profitability, making them stand out from existing nuclear power reactors.

Six main types of reactors were selected for further research and development and subsequent implementation: Gas-cooled fast reactor (GFR), Lead-cooled fast reactor (LFR), Molten salt reactor (MSR), Sodium-cooled fast reactor (SFR), Very high temperature reactor (VHTR), Super critical water-cooled reactor (SCWR). Operating temperatures for each type of reactor are: GFR – 850 °C, LFR – 480…800 °C, MSR – 700…800 °C, SFR – 550 °C, VHTR – >900 °C, SCWR – 510…625 °C [2]. It is important to note that the majority of operating industrial reactors practically do not have a coolant temperature above 350 °C. Therefore, the predicted operating conditions for Gen-IV systems pose significant challenges in the choice of construction materials. Structural components will be exposed to different operating conditions: exposure to higher temperatures, higher doses of neutrons and extremely aggressive environments. However, it is also important to note that one material suitable for one Gen-IV design may not be suitable for similar applications in other reactors, depending on the operating conditions of the particular reactor.

Among the desired characteristics of structural materials of Gen-IV, the following can be noted: the in-core materials need to exhibit dimensional stability under irradiation, whether under stress (irradiation creep or relaxation) or without stress (swelling, growth); the mechanical properties of all structural materials (tensile strength, ductility, creep resistance, fracture toughness, resilience) have to remain acceptable after ageing; the materials have to retain their properties in corrosive environments (reactor coolant or process fluid); acceptable resistance to radiation damage (radiation hardening and embrittlement) at high neutron doses (10…150 dpa), helium embrittlement, etc.; high degree of chemical compatibility of structural materials and coolant, as well as fuel. Finally, processability, weldability, cost, and any other important aspects should be considered in the material selection process. All these requirements are related to the fundamental mechanisms of high-temperature degradation, such as phase instability, oxidation, radiation-induced segregation, etc.

Ferritic-martensitic (FM) steels are one of the candidate materials for the future generation of reactors [3–7]. Before the finding the irradiation-induced void swelling phenomenon [8] high chromium (9…12 wt.% Cr) FM steels were used in the petrochemical industry, and later for gas turbines and conventional fossil fuel power plant applying [9, 10]. Firstly FM steels were not considered as structural and cladding materials in the early nuclear reactors and conventional austenitic stainless steels were used as structural components in nuclear service, but when it was understood that swelling behavior is a key parameter for fast reactor core materials selection [11–13] it became obvious that a scientifically based selection of new radiation-resistant materials is needed.

FM steels, especially containing 9…12 wt.% Cr (conventional Cr-Mo steels and the reduced activation ferritic-martensitic (RAFM) steels that differ from Cr-Mo steels due to W presence in substitution of Mo), exhibit excellent mechanical properties, thermal properties, irradiation tolerance, corrosion, and oxidation resistance [14]. These superior properties make the high Cr FM steels excellent candidates for Gen-IV reactors with several concepts proposed including GFR, SCWR, MSR, liquid metal cooled sodium fast reactors (Na-LMR) and lead fast reactors (Pb-LMR) [15, 16].

The reference FM steel considered for several reactor systems is the modified 9Cr-1Mo T91 steel. However, other FM steels, such as e.g. the Eurofer 97 and T92 steels, will be also included in GETMAT work programme [17]. Regarding to Europinean conception [18], FM steels are also considered as possible ATF materials as a cladding and core components where swelling must be low.

It was established that FM steels have higher swelling resistance [19] in comparison with the conventional austenitic stainless steels and that's why they were selected as materials for core components. In addition, it's well known that swelling of bcc-materials (Fe-Cr steels) typically is much lower than widely used austenitic base alloys. Moreover, swelling of steels with 9% Cr and which have mainly martensitic structure is lower than in 12% steels, structure of which consisted of both martensite and ferrite [20–22].

12Cr-1MoVW (HT9 grade) in the USA, unstabilized 9Cr-1Mo (EM10) and duplex 9Cr-2MoVNb (EM12) in France, 11Cr-MoVNbW (PNCFMS) in Japan, 12Cr-MoVNb (FV448, FV607, 1.4914) in the UK and Germany [23–29] were used for the fabrication of fuel assemblies irradiated in various fast reactors worldwide, among which EBRII (Experimental Breeder Reactor II) and the Fast Flux Test Facility (FFTF) in the USA, Phoenix and SuperPhoenix in France, Prototype Fast Reactor (PFR) in the UK. Because of their confined strength and creep efficiency at high temperatures (around 560 °C [9, 30]), this type of steels were mainly applied as wrappers (or ducts) in liquid metal cooled fast reactors where temperature did not exceed about 550 °C. Though, 12%Cr alloys HT9, FV448 and 9% Cr EM12 were used for cladding. Due to their excellent dimensional stability under irradiation, the use of FM steels as core materials in fast neutron reactors has been successful. Fuel assemblies made from FM steels have achieved high burnups with corresponding displacement doses on steels up to about 150…160 dpa [31, 32]. In particular, EM10 steel was chosen as wrappers material of Na-cooled fast reactors and for core components of other types of reactors: in ASTRID (Advanced Sodium Technological Reactor for Industrial Demonstration) [33], PNC-FMS steel for JSFR (Japan Sodium-cooled Fast Reactor) [34], CFR1000 (China Fast Reactor 1000) [35] and PGSFR (Prototype Generation-IV Sodium-cooled Fast Reactor) [36]. Another 12% Cr steel 15Cr12MoVWN was proposed for wrapper tubes in Chinese sodium-cooled fast reactors based on the requirements of tensile and creep strengths [37].

HT9 steel has been considered for both in-core and out-of-core applications of fast breeder reactors [38, 39], and for the first wall and blanket structures of fusion systems [40, 41]. Moreover, the HT9 steel has been applied fruitfully in the FFTF as fuel cladding and ducts [42]. HT9 steel was also considered as cladding material in LFR systems [43, 44].

9% Cr RAFM steel Eurofer 97 and its ODS versions is considered mainly for fusion reactors like DEMO as blanket, divertor cassette, structural material for the Water Cooled Lead Lithium concept of a fusion reactor and wall material [45–50]. Some other reduce activation steels were chosen for fusion systems: F82H and JLF-1 (Japan), OPTIFER Ia and OPTIFER II (Europe) and ORNL 9Cr-2WVTa (USA) [15].

FM steels are considered primary candidates for SFR cladding and duct materials of several Gen-IV SFR designs. The US fast reactor program adopted HT9. Similar types of steel have been chosen in Europe and Japan (EM12, DIN 1.4914, and PNC-FMS). In addition, T91 and T92 have also been chosen for similar application [7].

Worth a separate mention the modified 9Cr-1Mo steel with additions of Nb, V, and N (i.e. mod. 9Cr-1Mo or Grade 91/T91) which was developed in the 1970s [51, 52], in the first instance for SFR steam generator application and then as sole material for the sodium transport system [53]. T91 showed higher creep strength than standard commercial alloys in the range 2.25Cr-1Mo to 12Cr-1Mo [51] due to presence of fine V, Nb carbonitrides that arise during normalization and tempering treatments. From 1980s T91 was used for boiler tubing applications [54] and in the power and petrochemical industries [54, 55] and for conventional power plants that were designed for higher temperatures than the preceding plants (up to 590 °C) [9]. Additionally it should be noted that FM steels have smaller thermal expansion coefficient and a better thermal conductivity than austenitic ones and this leading to lower thermally induced stresses, better thermal fatigue properties and therefore increased component lifetime.

In nuclear power application, T91 has been provided for the Steam Generator of the European Fast Reactor (EFR) project. Following the EFR project, T91 has been recently considered as a candidate for the steam generator of the ASTRID prototype [56]. Moreover, FM steels are possible candidate materials for a power conversion system based on the super-critical CO_2 Brayton cycle [57].

T91 has also been chosen to manufacture the steam generator in the Prototype Fast Breeder Reactor [58] and Commercial Fast Breeder Reactors. Also, T91 was chosen as structural material for the primary and secondary heat transport system components (piping, intermediate heat exchanger and steam generator) of JSFR [59, 60].

LFR are fast spectrum reactors cooled by molten lead (or lead-based alloys) operating at high temperatures [61]. Liquid Lead or liquid Lead-Bismuth eutectic (LBE) were also chosen as coolant for several concepts of Accelerator Driven Systems (ADS). ADS are subcritical nuclear systems developed for different applications, in particular the transmutation of nuclear waste [62, 63]. FM steels have been selected, or considered as possible candidate materials for structural and core materials of

various LFR and ADS concepts. The materials performance assessment in heavy liquid metals has focused on FM and austenitic steels and the experiments have been conducted mainly in LBE. In particular, the FM steel T91 was chosen as one of the candidate materials for internal structural components of future LFR and ADS, because of its very good behaviour under irradiation and better corrosion resistance than austenitic steels. The proton beam window of the MEGAPIE (MEGAwatt Pilot Experiment) LBE spallation target, the first liquid metal target was made of T91 [64, 65]. T91 was also considered as wrapper and possibly cladding material for the lead-cooled ELFR (European Lead Fast Reactor) and ALFRED (Advanced Lead Fast Reactor European Demonstrator, a smaller size LFR demonstrator) [66–68] as well as for the wrapper, core support plate and spallation target window of MYRHHA (Multi-purpose hybrid research reactor for high-tech applications), an accelerator-driven LBE cooled system designed to operate both in subcritical and critical modes [69, 70].

The primary reference material for the hot vessel of reactor pressure vessel option is Grade 91. A substantial database on the baseline mechanical properties of the Grade 91 steel is currently available. Sufficient data are also available on the long-term thermal aging effects on the mechanical properties for this steel. However, additional data are needed for the mechanical properties of thick sections, where there is the possibility of retained ferrite in this martensitic steel that can lead to embrittlement. As with the other alloys under consideration, properties in impure helium must also be explored. Grade 91 is a relatively mature material, as indicated by its inclusion in Section III of the ASME Boiler and Pressure Vessel Code (BPVC), including in subsection NH on high-temperature materials. Code qualification applies for operation to 300000 h, whereas the current design concept of 60 years would require over 420000 h, if operated at 80% efficiency [71].

Gas-cooled systems studied in the framework of Gen-IV are the GFR and the VHTR. However, European materials research programmes for the gas cooled reactors have focussed on the VHTR concept [72–74]. T91 steel is a candidate material for the hot reactor vessel [75] of the gas-cooled Gen-IV systems, which should operate at temperatures close to ~ 450 °C on condition if no separate cooling circuit is provided in the reactor design. So far, no reactor vessel using 9Cr FM steels has ever been built.

The concept of SCWR is also considered FM steels as structural materials. A number of the FM steels was found to have better stress corrosion cracking resistance in SCW than other classes of metallic alloys, however due to their poorer corrosion behavior, they are probably less suitable for use in a SCW environment [76, 77].

Finally FM steels such as HT9 are foreseen to be used as wrapper and cladding materials for the Travelling Wave Reactor (TWR), a sodium cooled "breed and burn" fast reactor concept [78]. But it is important to note that TWR have much higher peak doses (~ 600 dpa) in comparison with Gen-IV systems (~ 200 dpa). This push towards very high damage levels in revolutionary nuclear systems has sparked in recent years numerous irradiation experiments of FM steels to several hundreds of dpa using ion beams, with the aim to investigate the microstructural evolutions occurring at very high damage doses, in terms of swelling, intergranular segregation and precipitation behaviors [79–82].

A particular class of materials should also be noted – oxide dispersion strengthened (ODS) FM steels. ODS FM steels are considered for cladding materials for high burn-up fast neutron reactor fuels (especially MA956 and PM 2000). The nanosized dispersoids of yttrium oxide give these alloys a good creep resistance at high temperatures [83]. The ODS grades currently developed in the frame of the SFR or fusion contain 9…12% Cr. However, these alloys could show some limitations in terms of internal corrosion (oxide clad reaction) and temperature (phase transition around 1075 K). Therefore, ferritic steels with ~ 14% Cr and more could be used up to 1175 K.

As noted above, FM steels have high-temperature mechanical characteristics limited to ~ 500 °C (heat resistance, thermal stability, creep, etc.), while the operating temperatures of new generation reactors are much higher [7]. Moreover, in 12% Cr steels, there is a problem of δ-ferrite formation, which can degrade the mechanical properties, especially after irradiation. It should be noted that microstructure, not crystal structure, is the dominant characteristic that determines swelling of FM steels [84]. But when using thermomechanical (TMT) and heat (HT) treatment, these disadvantages can be avoided. Furthermore, namely structure and mechanical properties determine the safe and economical functioning of nuclear systems.

This review discusses the methods of thermal and thermomechanical treatment, microstructure features and mechanical characteristics of FM steels that will be used in future generations reactors.

1. TREATMENT METHODS OF FM STEELS

The standard HT of FM steels is normalization in the austenite stability region (≥ 1040 °C) and tempering at temperatures below the A_{C1} point (> 700 °C) [85–87]. The received state after the standard HT is usually called "N&T".

Thermal and thermomechanical treatment of steels and alloys are used for structure modernization and improving of mechanical, physical, radiation and other properties [88–91].

Among the main methods of HT austenization, partial and short-term tempering, additional quenching, etc. are noted. The most common TMT methods are ausforming, rolling (cold and hot), equal channel angular pressing (ECAP), high pressure torsion, overall forging, etc.

While HT mainly leads to an improvement in the structural features of materials due to phase transformations, TMT makes it possible to qualitatively improve both the structural and mechanical characteristics of metals and alloys. TMT increases the strength properties of materials while maintaining a sufficient level of ductility. Thus, after TMT, the strength of the material increases both as a result of cold-hardening formed during plastic deformation and as a result of quenching. Due to this, during TMT it is

possible to achieve higher hardening than during conventional quenching.

At the same time, 9% Cr steels are recommended to be subjected to TMT, mainly to improve the characteristics of high-temperature strength and stability, while for 12% Cr FM steels, it is necessary to apply HT that should be used to prevent the formation of δ-ferrite, which negatively affects the mechanical characteristics of this type of steels. But for 9% Cr FM steels, HT is also provided for the modernization of the structure before the following TMT.

Moreover, the mechanical properties of FM steels are critical and important for the practical applications at elevated temperatures, especially in nuclear application.

Various strengthening approaches have been used to improve the strength of FM steel, among which precipitation hardening and strain hardening have much influence on mechanical properties at elevated temperatures. Normalizing and tempering temperature strongly influences the shape and size of second phase precipitate particles (i.e. $M_{23}C_6$, MX). Additionally, severe plastic deformation (SPD) technique, which causes refinement of grain size up to nano-scale, increase in dislocation density and increase in number of precipitates with several order of magnitudes. It also imparts significant hardening of martensite and fine distribution of second phase particles. These second phase particles can stabilize the microstructure by pinning the grain boundaries and restricting the motion of dislocations to assure high temperature strength. The main shortcomings of actual 9…12% Cr high-chromium steels are that the creep resistance is not enough to fulfill the engineering requirements at temperatures higher than 600 °C and the material undergoes a cyclic softening. Creep strength at high temperature could be improved by a microstructural optimization through nano-precipitation, guided by computational thermodynamics, and thermomechanical control process optimization [3, 15].

Let us consider data on different modes and methods of thermal and thermomechanical treatment of FM steels. In the following sections, the effect of these treatments on the mechanical properties and structure of 9…12% Cr steels will be presented.

To study the effect of HT on microstructure and hardness of Grade 91 steel [92] normalizing was first done on each sample within a temperature range of 1020…1100 °C for 2, 4, and 8 h. Normalizing temperature and time were so chosen that austenitization had been complete before tempering was carried out. Normalized samples were air cooled (AC) down to room temperature before tempering at various temperatures and times. Samples that have been normalized at 1040 °C for 2, 4, and 8 h were tempered at 690, 725, 745, and 790 °C for 2, 8, and 20 h. Tempering of samples normalized at 1040 °C for 2 h was expanded to include temperatures in the range of 635…850 °C. This created a matrix of close to 50 possible combinations of normalizing and tempering scenarios, which provided an adequate sequence to reveal the microstructural changes during HT.

Heterogeneous grain growth during austenitization in ASTM A213-T91 steel has been studied in [93]. The material was received in its standard condition, that is, normalized at 1060°C and tempered 40 min at 780 °C. The thermal cycles were carried as follows: heating at a rate of 1 and 50 °C/s, austenite holding at 1060 and 1080 °C for 1, 15, and 30 min and quenching at 50 °C/s.

The microstructural parameters (dislocation density, martensite lath width, precipitate diameters and volume fractions) have been investigated for the 9% Cr steel P92 (NF616) after 2 h at 1070 °C of austenitising and 2 h at 715, 775, 835 °C of tempering (to increase degrees of martensite recovery and decrease dislocation density), 2 h at 970 and 1145 °C of austenitising and without or with tempering at 775 °C for 2 h (to increase prior austenite grain size) and 2 h at 1070 °C of austenitising with furnace cooling (FC) to 780 °C and subsequent tempering at 780 °C for 8 h with FC to room temperature (to receive ferritic matrix with no martensitic transformation) [94].

Very interesting method of thermal treatment (namely – partial tempering) is proposed in [95]. This modified HT method is used instead of TMT to achieve high mechanical characteristics. All the partially tempered (PT) samples were processed by normalizing the as-received (AR) T91 steel at 1000 °C for 15 min with AC and a subsequent partial tempering treatment at 300, 400, 500, 600, and 700 °C for only 3 min followed by water cooling. A detailed scheme of thermal treatment is shown in Fig. 1.

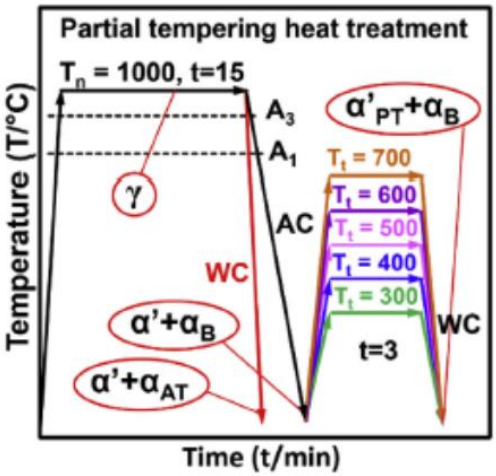

Fig. 1. The heat treatment procedures for T91 steel. AC – air cooling, WC – water cooling [95]

The influence of HT on structure and tensile properties of 15Cr12MoVWN (HT9 type) FM steel was determined in [96]. HT regeimes were as follows: Austenitizing at 1000, 1050, and 1080 °C, tempering at 650, 700, and 760 °C with next water quenching (WQ), oil quenching or AC.

In [97] to assess the failure resistance of HT9 specimens were heat treated to twenty-five combinations of austenitization temperature. Each HT consisted of austenitizing at one of five temperatures for one hour, followed by AC and then tempering at one of five tempering conditions followed by subsequent AC. The austenitizing temperatures (Tγ) were 950, 1000, 1050, 1100, and 1200 °C. The tempering conditions were 650 °C – 1 h, 650 °C – 56 h, 715 °C – 1 h, 735 °C – 0.5 h, and 780 °C – 1 h; the corresponding

tempering parameters (P_T = T(K) (logt(h) + 20) × 10^{-3}) ranged from 18.5 to 21.

The effects of the HT conditions on the microstructure and mechanical properties of HT9 steel were studied in [98]. The HT9 steel was normalized at 1000 to 1100 °C for 30 min followed by AC to room temperature. The tempering treatment of the normalized specimens was carried out at 700 to 780 C in 1 h followed by AC to room temperature.

Effects of HTs, with varying normalizing temperature, temper temperature and cooling rate, on the microstructure and mechanical properties were studied in [99]. To investigate the effect of normalizing temperature on grain size, hardness and grain boundary misorientation, Eurofer ODS steels were subjected to solution treatment at 980, 1040, 1100, 1150, 1300, and 1350 °C, followed by cooling and tempering at 700 °C; T92 and Eurofer 97 steels were subjected to solution treatment at 980, 1040, 1100, and 1150 °C, followed by WQ and AC, respectively, and tempering at 700 °C. Different cooling rates, WQ, AC, and FC are applied to Eurofer ODS steels to observe the effect on grain boundary misorientation. Eurofer ODS and T92 were subjected to solution treatment at 980 °C, followed by WQ, and tempering at 550, 650, 750, and 850 °C.

Regarding TMT – in [100] the Eurofer 97 plate was hot deformed using two reheating conditions (1075 and 1175 °C). Two finish rolling temperatures (750 and 650 °C) and two different total reductions (30 and 40%) are also analyzed. The tempering effect is also studied (in the temperature range 720…760 °C).

Another study of the effect of ausforming of Eurofer 97 steel on structure and mechanical properties described in details in [101]. Here the TMT consisted of a solution and austenitization treatment at 1250 °C in air followed by cooling in a second furnace. The temperature of the second furnace was set to the desired rolling temperature (namely 600, 700, 800, and 900 °C).

To study microstructural and mechanical characteristics of Eurofer 97 specimens in the AR condition were ECAP processed at 550 °C through a die with an intersection angle of 105° [102]. The billet was rotated around its longitudinal axis before inserting in the die for the following ECAP pass, either 180° (route C) or +90° and -90° alternatively (route B_A). The billets were subjected to 1, 2, and 4 ECAP passes following route C, as well as 8 passes following route B_A.

Guidelines for tailoring the microstructure and mechanical properties of T91 steel via ECAE (equal channel angular extrusion) enabled TMT for an improved combination of strength and ductility are presented in [103]. TMT processes include: (1) austenitizing at 800…1200 °C (with an interval of 100 °C) for 1 h followed by quenching in ice water; (2) ECAE process of austenite at 1000 °C followed by WQ, and then tempering the thus- deformed T91 steel for 1 h at 300…800 °C; (3) tempering the water quenched specimens at 500 °C for 10 h, followed by ECAE of the tempered specimens. ECAE was carried out with number of extrusions from 1 to 3 at room temperature, 300 and 700 °C.

Effect of normalizing (950…1050 ºC) and tempering (650…700 ºC) has been investigated to study the microstructure and mechanical properties of modified 9Cr-1Mo steel (G91) [104]. To improve the high temperature mechanical properties, hot rolling has been done at optimized normalizing and tempering conditions. The hot rolling is carried out in three passes at 1050 and 550 ºC.

In [105] to refine the 9Cr-1Mo martensitic steel (T91) it was processed by ECAP method at room temperature and annealed at 500 °C for 2 h subsequently. ECAP processing was carried out in a self-designed die with the intersecting angle of 120° with an amount of extrusions from 1 to 6.

A brand new method of deformation of 9…12% Cr steels is proposed in [106]. The microstructure and mechanical properties of the FM steel T91 after SPD and subsequent thermal treatment was investigated. SPD was realized by the original method, developed in NSC KIPT of multiple "upsetting-extrusion" (MUE) [107], in temperature range of stability of ferritic phase (750…575 °C), thermal treatment of SPD specimens was carried out at temperatures 550…730 °C during 1…100 h.

Effects of ausforming through upsetting and following tempering on microstructure and mechanical properties under uniaxial tension of 12CrWMoNbVB FM steel are studied in [108]. TMT included heating in air to ~ 890 °C, holding at this temperature for 15 min, and following upsetting (i.e. ausforming). After that the samples from the ausformed steel were tempered in an argon atmosphere at three modes: 720 °C for 3 h; 665 °C for 3 h; 550 °C for 25 h, with further cooling of the samples in the air.

2. MICROSTRUCTURE OF FM STEELS

After standard HT, all 9…12% Cr FM steels have a tempered martensite structure. It necessarily contains prior austenite grain boundaries (PAGB) decorated with carbides of the type $M_{23}C_6$ (where M – Cr, Fe, W). In the body of the prior austenite grains (PAG), carbides and/or carbonitrides of the MX type are uniformly distributed (where M – V, Nb, Ta and X – C, N). Generally, the sizes of $M_{23}C_6$ precipitates are 60…200 nm, while MX – ≤ 50 nm [109–113]. The mean grain size according to [86, 96, 114] is ~ 20 μm. But if the Eurofer 97 and T91 steels are supplied as a hot rolled plates, they present a fine structure with a PAG size in the ASTM range 10…11.5 (6.7…11 μm) for the 14 mm plate and ASTM 10.5…11 (8…9.4 μm) for the 25 mm thickness plate [92, 115, 116].

The typical view of 9…12% Cr steels structure is presented on Fig. 2. It can be seen that 9% Cr steels have a pure martensitic structure, while 12% Cr contains δ-ferrite in the form of white islets and streaks. Because of its higher chromium (a ferrite stabilizer) content, HT9 can contain 0…2% δ-ferrite, depending on composition variations within the alloy specifications (see Fig. 2,c). It is generally believed that the effect of δ-ferrite in 9…12% Cr FM steel on properties depends on its volume fraction. Hu et al. [117] and Hu [118] show that, in the steel E911, δ-ferrite has little effect on the strength of steel. When the volume fraction of δ-ferrite is smaller than 0.3%, it can slightly increase the strength of steel. A small amount of δ-ferrite (less than 1%) does not affect

the properties of steel, and can even improve the ductility and toughness of steel to a certain extent. Only when it is over 1% is a bigger impact produced in the fracture toughness of the steel.

Also, the ferrite phase inhibits austenite grain growth, but it adversely influences the strength and, directly or indirectly, the toughness [119–121], particularly if present as films between the grains of the austenite, which is subsequently transformed to martensite and tempered. That's why steels with 9% Cr were favored over those with 12% Cr because of the difficulty of eliminating δ-ferrite in a 12% Cr steel without increasing carbon or manganese for austenite stabilization and specific heat treatment, but manganese promotes chi-phase precipitation during irradiation, which can cause embrittlement [15].

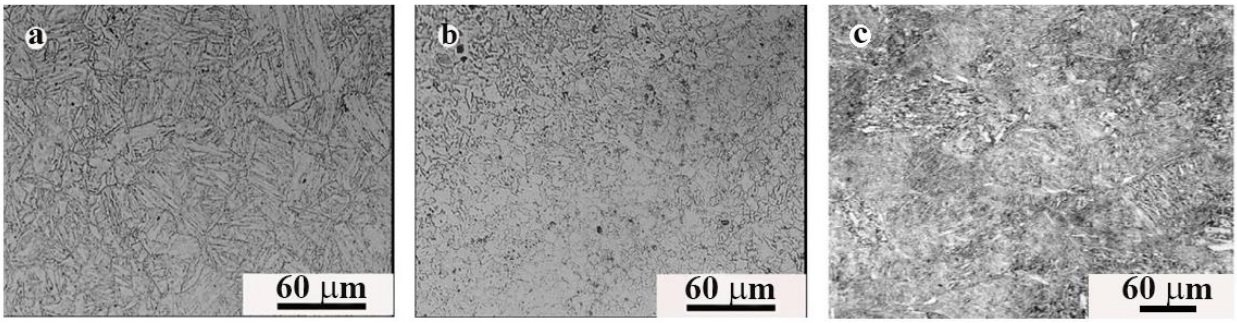

Fig. 2. Microstructure of initial T91 (a); Eurofer 97 (b) [122], and HT9 (c) [84] steels

After HT and TMT, the structure of 9…12% Cr steels changing. Thus, after normalizing time of 2 h, PAG size and martensite lath size increased with increasing normalizing temperatures of 1020…1100 °C for steel T91. The as-normalized (1040 °C for 2 h) microstructure had hard martensitic lath structures with high dislocation density and for constant normalizing temperature of 1040 °C, martensite lath size and PAG size increased with increasing normalizing time of 2, 4, and 8 h. Grain size increased with increasing normalizing time, and tempering time. The sample normalized at 1040 °C for 2 h and tempered at 790 °C for 2 h has grain size of ~ 11 μm, while sample normalized at 1040 °C for 8 h, and tempered at 790 °C for 20 h resulted in a grain size of ~ 17 μm. The grain size of initial steel was ~ 7 μm [92]. The obtained structures are given on Fig. 3.

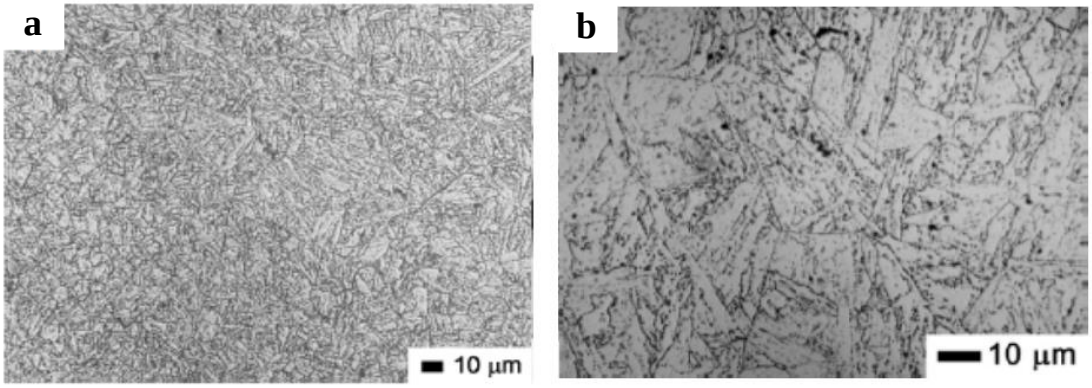

Fig. 3. Microstructure of T91 steel: a – initial; b – normalized at 1040 °C for 8 h and tempered at 790 °C for 20 h [92]

Heterogeneous grain growth during austenitization in T91 steel has been investigated in [93]. Starting from a uniform, fine austenite grain size distribution after 1 min of holding time, a heterogeneous austenite grain size distribution was observed after 15 min of holding time at 1060 and 1080 °C and it was relatively insensitive to the change in the heating rate. This heterogeneous growth is probably related to the evolution of MX precipitates during the austenite treatment. For the 1 min of annealing, precipitates were found to be Nb-rich MX (major) and V-rich MX (minor), these last with sizes higher than 50 nm. Very few $M_{23}C_6$ particles were also detected. For the 15` and 30` of annealing times V-rich precipitates were not found, and the chemical composition of the Nb-rich precipitates displayed values slightly higher than those measured in the AR state. M_3C precipitation was not observed to be related to MX precipitation; on the contrary, zones with MX presence and no M_3C particles were marked. On the other hand, M_3C precipitates are mainly found in coarse martensite laths, a similar observation has already been reported in [123] for the T92 steel.

Some interesting results were obtained in [94]. Thus, increasing of tempering temperature for P92 steel leads to enhanced martensite recovery processes, which decrease the dislocation density. These processes were accelerated at higher tempering temperatures, so that tempering at 715 °C led to a slightly higher dislocation density than the standard tempering at 775 °C. Tempering at 835 °C caused a sharp decrease in the dislocation density of about 75%. With increasing austenitising temperature the austenite grain size and the martensite lath width increase (lath – from 0.38 nm at 970 °C to 0.42 nm at 1070 °C, and 0.58 nm at 1145 °C;

grain size – from 10 μm at 970 °C to 20 μm at 1070 °C, and 60 μm at 1145 °C). The dimensions of the larger $M_{23}C_6$ and the fine MX precipitates were similar for all three HT conditions.

The untypical, for initial state, phases are observed in T91 steel structure after partially tempering [95]. The AR sample is shows a typical fully tempered martensite (α'_T) microstructure with a large number of coarsened precipitates distributed along PAGBs and martensitic lath boundaries, indicating a significant release of carbon atoms from the matrix. The microstructure of 1000WQ sample (normalizing at 1000 °C for 1 h, followed by WQ) consisting of a majority of quenched martensite (α') and a small amount of auto-tempered martensite (α'_{AT}) formed during the cooling process. Relatively clean (precipitate-free) PAGBs and lath boundaries indicate that most carbon atoms are dissolved into the matrix forming supersaturated quenched martensite. A certain amount of coalesced bainitic ferrite (α_B) (labelled by yellow dash line on Fig. 4) and partially tempered martensite (α'_{PT}) were discovered in the PT T91 samples, as shown in Fig. 4. The microstructure of the PT T91 steel consists of partially tempered martensite and bainitic ferrite with transition carbides and ultra-fine martensite. The transition carbides within the bainitic ferrite grains in the PT samples are identified as ε- and θ-carbides, and ε-θ-carbide complexes.

The microstructures of 15Cr12MoVWN steel after austenitizing at 1000, 1050, and 1080 °C, tempering at 650, 700, and 760 °C with next WQ, oil quenching or AC is investigated in [96]. It is observed that 15Cr12MoVWN steel has a fully martensitic structure without formation of δ-ferrite after all HT regimes. The average grain size varies little with the different cooling methods and tempering temperatures. On the contrary, the PAG size changes obviously with different normalizing temperatures, especially for normalizing at 1080 °C. The higher the normalizing temperature, the greater the grain size. The normalizing temperature is therefore the most important factor affecting the PAG size among the influencing factors in the orthogonal design experiment.

Fine martensitic laths dominated in the specimens tempered at 650 and 700 °C irrespective of the normalizing temperature and cooling method. When the tempering temperature increased to 760 °C, the dislocation recovery accelerated, and the dislocations in the martensitic lath passed through the precipitates by climbing or bypassing to form a dislocation wall, which promoted the formation of subgrains and accelerated the crushing of the lath. The increasing tendency of the martensitic lath width is low from 650 to 700 °C, but significant at 760 °C during tempering. The lath width increased with increasing grain size and normalizing temperature. The tempering temperature was more effective in adjusting the lath width than the normalizing temperature. The present results of lath width variation in the 15Cr12MoVWN steel specimens are in good agreement with the literature [124].

Two types of precipitates were observed in 15Cr12MoVWN steel. The elongated precipitates $M_{23}C_6$ distributed in the chain along the grain boundaries, whereas fine spheroid particles MX distribute predominantly in the laths.

The HT9 cladding tube has a typical martensite structure, and the PAG size increased with an increase of normalizing temperature [98]. The microstructure of the normalized specimens consisted of lath martensite with a high dislocation density due to austenite to martensite transformation. The tempered specimens showed a tempered lath martensite structure with a low dislocation density because of the dislocation recovery. The lath width is not greatly affected by the tempering temperature change. A precipitate, unlike a lath structure, varies depending on the tempering temperature.

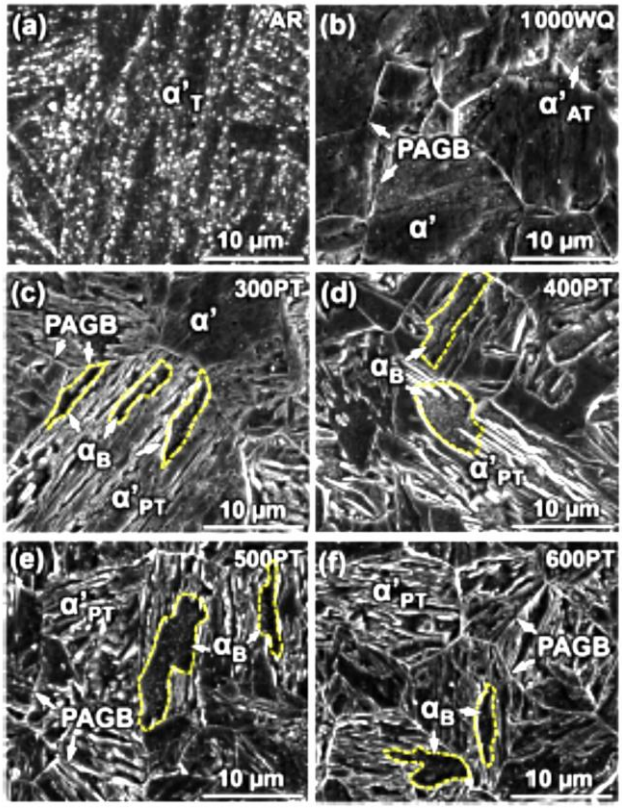

Fig. 4. SEM micrographs of the AR, WQ, and PT T91 specimens heat treated at 300…600 °C: a – AR T91 steel; b – WQ sample; c–f – PT samples [95]

Fig. 5 shows the precipitates and PAG size, as well as the lath width according to the tempering parameter (i.e. Hollomon-Jaffe parameter). The PAG size indicates a similar value by increasing the tempering parameter. The PAG size was not affected by the tempering parameter. It is known that PAG size varies with the normalizing temperature. The lath width showed similar values by increasing the tempering parameter. The lath width was not affected by the tempering parameter. However, the size of the precipitate was increased by increasing the tempering parameter. The precipitate behavior was affected by the tempering parameter.

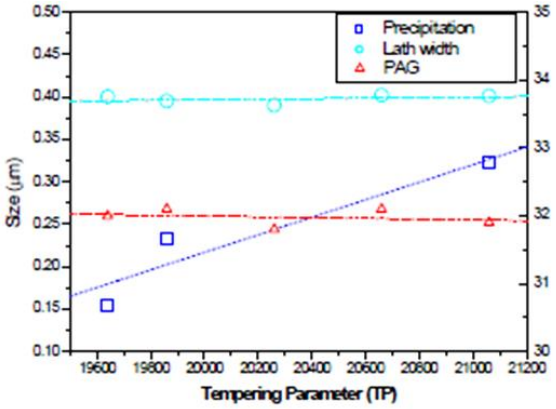

Fig. 5. Tempering parameter with the lath width, prior austenite grain size and precipitation mean size at 1050 °C [98]

Effect of HT on microstructure of Eurofer 97 steel, two Eurofer ODS variants (HXX and FZK, the latter having a very low carbon concentration) and T92 (or NF616) is studied in [99]. Thus, for T92 and Eurofer 97 steels, the grain size increases with the increase of solution temperature. The grain coarsening rate of T92 is faster than that of Eurofer 97. This may be because there is higher Ta concentration in Eurofer 97 than Nb in T92 (both Ta and Nb play a role of grain refinement). In Eurofer ODS steels (HXX and FZK), the grain size remains almost unchanged up to 1300 °C. After that, grain size increases with the increase of normalizing temperature. This indicates that the pinning of grain boundaries by yttria (Y_2O_3) particles is effective below 1300 °C. The dependence of PAG size on normalizing temperature is shown in Fig. 6.

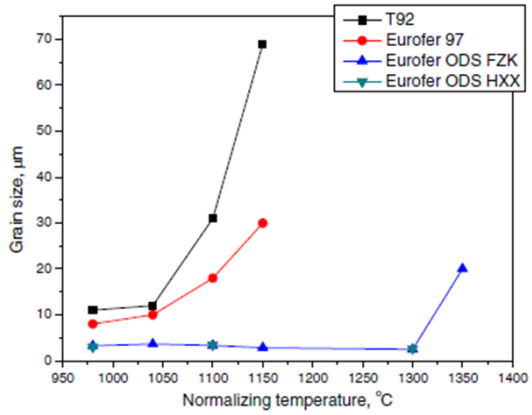

Fig. 6. Prior grain size vs. normalizing temperature [99]

A strong effect of reheating temperature before TMT on austenite grain growth is detected [100]. Hence, after heating at 1075 °C, subsequent hot rolling at 750 °C (hot reduction was 40%) and next tempering at 720 °C the structure of the Eurofer 97 sample is similar to tempered martensite with fine prior austenite grains (Fig. 7,a). But after heating at 1175 °C, hot rolling at 650 °C (hot reduction was 40%) and tempering at 720 °C the dramatically grain growth is observed and the form of the structure changes significantly (see Fig. 7,b).

Another variation of ausforming of Eurofer 97 was performed in [101]. The microstructural investigations showed large and elongated primary boundaries. Neither of the materials exhibited a full martensitic structure. Despite the annealing at 750 °C for 2 h, a high density of dislocations still observed. With increasing of rolling temperature, the martensite laths and secondary phases were refined. After rolling at 900 °C a larger amount of fine precipitates (10…20 nm diameter) inside the subgrains was observed. Also a reduction of the particle agglomeration with increasing of TMT temperature was detected. Agglomerations of fine MX precipitates were only observed in the materials rolled at 600 °C. Coarse $M_{23}C_6$ carbides a representinall material due to the carbon content of 0.1 wt.%. Their size and shape were not affected by the rolling conditions. $M_{23}C_6$ particles with a typical sizes range between 100 and 300 nm were measured in all cases.

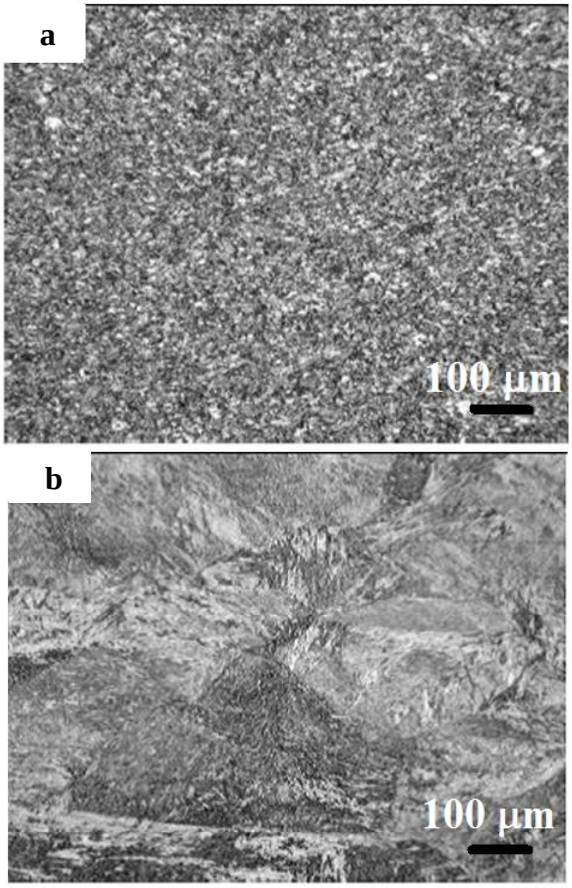

Fig. 7. Effect of reheating temperature on microstructure of Eurofer 97 steel: a – after reheating at 1075 °C; b – after reheating at 1175 °C [100]

The effect of ECAP on the microstructure of tempered Eurofer was studied in [102]. The microstructure of the AR samples exhibited traces of the PAGs and martensite laths. Furthermore, carbide particles were found homogeneously distributed in the matrix, as well as located at PAGBs and along the lath boundaries. After the first ECAP pass the microstructure exhibited large elongated grains fragmented into subgrains, as expected. This fragmentation may be due to dislocation arrangement into walls and cells induced by the dynamic recovery mechanism during the ECAP process at 823 K. Note that some subgrains are separated by a dislocation wall and other subgrains seem to have developed from a dislocation cell. After the fourth pass, the microstructure was no longer elongated, martensite laths were not observed and an equiaxed structure of

submicron grains appeared, but still the number low angle grain boundaries was abundant. Eight passes via route B_A generated a more refined structure, with grain sizes less ~ 500 nm and a high number of high-angle grain boundaries.

TMT by ECAP method of T91 steel was carried out in [103]. The as-annealed (so-called AA, annealing of AR material at 800 °C for 1 h, followed by FC) T91 steel has typical tempered martensitic lath structure ($\alpha`_T$) with minor second phases, including retained austenite or martensite (M/A constituent), and/or transformed carbides. The fully tempered T91 is mainly composed of ferrite phase with packet and block boundaries. PAGBs and packet boundaries are often decorated by "white" carbide particles. Tempered martensite laths in the AA specimen dominate the microstructures inside a packet.

WQ of T91 from 800 °C (specimen called 800WQ) leads to fine microstructure and it is shown that this fine structure is a mixture of grain boundary ferrite (α_A), martensite ($\alpha`_M$), and polygonal ferrite (α_P). Some martensitic blocks within PAGs were etched. A PAG in the 800WQ specimen is surrounded by adjacent α_A containing undissolved carbides. The ferrite phase (α_P) and fine martensite are occasionally separated by a packet boundary.

The microstructures of the water quenched 900 and 1000 °C specimens (900WQ and 1000WQ, respectively) have primarily martensite $\alpha`_M$ and polygonal ferrite (α_P), α_A is absent in the 900WQ specimens. PAGBs are also observed in the 900WQ specimen and a triple junction of PAGs in the 900WQ T91 is observed. Retained austenite γ is identified as the thin layers between martensite laths with dark contrast. The α_P ferrite with martensite precipitates is also observed in the 900WQ specimen.

Significant coarsening of austenite grains occurs after HT at 1100 °C or higher prior to WQ as was detected in the 1100WQ and 1200WQ specimens. Blocks are clearly observed in these two specimens. Except for packets around the grain boundaries, no packet boundaries are identified due to the randomly oriented blocks. Bainitic ferrite (α_B) within the prior austenite grains in the 1100WQ and 1200WQ specimens was preferentially etched away. Auto-tempered martensite ($\alpha`_{AT}$) is frequently observed in the 1200WQ specimen. Carbides formed within the martensite laths.

The grain sizes of the PAGs in the WQ T91 steel are similar ~ 13 μm in the AA, 900WQ and 1000WQ specimens. For specimens heated to 1100 °C or greater (1100WQ and 1200WQ), the average grain size increased by an order of magnitude from ~ 13 to 150 μm.

Carbides in auto-tempered martensite and bainitic ferrite were also studied. Black needle-shape precipitates are identified in the specimen 1200WQ as η-carbide and cementite. Precipitates in bainitic ferrite align along nearly the same direction, in comparison to randomly oriented precipitates in auto-tempered martensite in the 1200WQ material and were identified to be ε-carbide.

It can be observed that such phases as auto-tempered martensite, bainitic ferrite etc. formed in 9% Cr steels after WQ [95, 103]. However, the effect of these phases on radiation resistance, mechanical properties after long-term servicing in environments with elevated temperatures, corrosion and erosion resistance is almost not studied. That is why a more detailed study of the properties of FM steels after this type of quenching is required.

The influence of HT and TMT by hot rolling on dislocation density, grain and precipitates size of T91 steel studied in details in [104]. The average packet size of initial steel is found ~ 15 μm, which is reduced to 5 μm in a sample, normalized at 950 °C and tempered subsequently. This indicates that the packet size is strongly dependent on the normalizing temperature. Hot rolling with 27% deformation causes reduction in the packet size up to 10.7 μm.

The variation of particles size at the grain boundary and grain interior under various HT and hot rolled conditions was presented. In AR state, the average size of particles at the grain and within grain boundary is found to be (250 ± 34) and (180 ± 20) nm, respectively. The particle size is observed to decrease with the increase in normalizing temperature (950…1050 ºC). Particle size increases at the PAGBs and within grains with the increase in tempering temperature. In order to optimize the size of precipitate particles to achieve high strength and ductility, tempering is performed between 650 to 750 ºC. There is a decrease in precipitate size with the low tempering temperature, which results into high stability of lath boundaries by $M_{23}C_6$ particles at elevated temperatures and less dislocation recovery. The particle size is found to be minimum for R550-T650 (where R – rolling, T – tempering), which is (95 ± 20) nm along grain boundary and (77 ± 19) nm within grain. The small particle size provides better pinning effect and hinders the movement of dislocations, which leads to an increase in the mechanical strength at room temperature and 650 ºC. At elevated temperature, high rate of self-diffusion of iron atoms and gliding of dislocations cause deformation and vacancies formation. In order to prevent the movement of dislocations, sufficient number of precipitates are required for the improvement in high temperature mechanical strength.

After normalization at 1050 °C and tempering at 750 °C the structure is typical tempered martensite with martensitic lath of 100…400 nm width, where $M_{23}C_6$ particles decorates the lath boundaries and have average diameter of about 150…300 nm. Additionally, average diameter of fine carbides is observed as 15…40 nm within the matrix. If normalized at 1050 °C and tempered at 750, 700, 650 °C the precipitate size changes significantly with the decrease in tempering temperature. Additionally, lath width and precipitates ($M_{23}C_6$/MX) increases with the increase in tempering temperature.

Similar behavior of precipitate size can be observed after hot rolling at 550 °C and tempering at 650 °C (i.e. R550-T650). It shows the formation of dislocation cells and decrease in lath size (~ 150…300 nm) as compared to other heat-treated conditions. High dislocation activity causes formation of dislocation forests. The higher extent of decrease in precipitate size and lath width significantly improved the mechanical properties at room temperature and 650 °C. The precipitate encircled in R550-T650 condition confirms the Cr-rich $M_{23}C_6$ carbides.

The microstructure of AR T91 steel and after ECAP is investigated in [105]. Compared with the initial material (average grain size ~ 20 μm), after one extrusion

pass, martensitic laths are destroyed and grains are broken. The grain elongation gradually becomes evident and the grain boundaries become more and more hazy until invisible with the increase of extrusion passes. The results indicate that due to plastic deformation the microstructure is severely distorted.

The microstructure of the initial sample contains arrays of martensitic laths with a width of ~ 0.4 μm and there are a certain amount of dislocations distributed in the matrix. Furthermore, some second-phase particles are found to disperse in the martensite borders and grain boundaries. For the sample after one pass, it is difficult to observe complete martensitic laths. However, many deformation bands in the martensitic laths, as well as lots of dislocations can be observed, which may be regarded as the formation of dislocation cells [125–128]. With the increase of extrusion passes, a number of dislocations will be introduced and pile up and eventually form new low-angle boundaries. The equiaxed and refined grains are formed after six passes, where most of the grain boundaries are of high angle type. In addition, there are high density dislocations in the grains and get tangled together in different places. After six passes the grain size is distributed in the range of 0…700 nm with the mean grain size of about 200 nm. So it can be concluded that the SPD such as ECAP can effectively refine the grains of T91 steel down to the nanometer scales.

To evaluate the thermal stability of the T91 steel refined by ECAP processing, the annealing was performed at 500 °C for 2 h for the ECAPed samples. The average grain sizes of the ECAPed samples after annealing are slightly larger than those before the annealing. For example, after annealing the average grain size for the sample after six ECAP passes has slightly grown up from about 200 nm to about 300 nm. In addition, the dislocation density in the samples after annealing is much lower than in the samples before the annealing. Therefore, the annealing at 500 °C mainly decreases the density of dislocations and results in very little grain growth.

The investigation of the microstructure after different number of "upsetting-extrusion" (UE) cycles showed that it is similar – well-formed grained microstructure with contrasting boundaries [106]. Increase in the number of cycles and decrease of UE temperature leads to the considerable decrease in subgrain size (from 5 μm to 145 nm) and to the improving of their size distribution uniformity. Decrease in mean subgrain size *d* with the increase in number of UE cycles occurs irregularly. Especially significant microstructure refinement is observed during deformation up to 3 cycles (e = 4.5). Herewith *d* decreases more than 10 times – from 5 μm in AR state to ~ 475 nm. With a subsequent increase in number of cycles from 3 to 5 (total deformation e = 8.0) value of *d* decreases approximately in 3 times – from ~ 475 to ~ 145 nm. Studies of precipitates size and density of deformed samples indicated that $M_{23}C_6$ precipitates density is practically independent on thermal treatment temperature and their mean size increases a few with the temperature increase, which is in agreement with the literature [92, 129]. Herewith density of MX precipitates is maximal ($2.0 \cdot 10^{21}$ 1/m^3) and size of precipitates is minimal (11 nm) after thermal treatment at 550 °C during 25 h.

Finally, after upsetting of a 12CrWMoNbVB steel at temperature of 890 °C with the true deformation of 0.7, a banding microstructure with a pronounced direction of deformation and a transverse size of subgrains of 260 nm is observed (vs. 220 nm in initial state) [108]. In some areas, there is no clearly pronounced direction, the grains are oriented chaotically. After tempering deformed specimens at 720, 665, and 550 °C a subgrain structure with an initial stage of recrystallization is observed, when, along with the formed larger grains with clear boundaries, practically without dislocations in the grain field, there are also subgrains of the initial state 5–7 times smaller in size. There are noticeably more areas with a smaller subgrain after tempering at 550 °C for 25 h than after tempering at 720 °C for 3 h. Regarding density of $M_{23}C_6$ carbides it was found that it varies slightly in all modes of HT and their size is in the range of 100…140 nm in initial state and after tempering at 720 and 665 °C, but reach 86 nm after tempering at 550 °C.

3. MECHANICAL PROPERTIES OF FM STEELS

As mentioned in the previous section, various types of HT and TMT lead to different changes in the microstructure of materials. The grain size, the present phases and the types of precipitates will affect the mechanical properties of the steels.

The main parameters of mechanical characteristics are yield strength ($\sigma_{0.2}$), ultimate tensile stress (UTS or σ_B), ultimate elongation (δ) and microhardness (HV). Below we consider the effect of HT and TMT on conventional and reduced activation FM steels.

Effect of normalizing treatment on Grade 91 hardness is studied in [92]. Hardness measurements were performed on the alloy samples normalized at 1020, 1040, 1050, 1060, 1080, and 1100 °C while keeping the time constant at 2 h. The hardness decreased with increasing normalizing temperature from 4000 MPa at 1020 °C to ~ 3500 MPa at 1100 °C. The hardness value was about the same for normalizing carried out at 1020 and 1040 °C, but after that, the hardness gradually decreased until reaching 1100 °C. The effect of change in normalizing time was studied by heat treating Grade 91 steel at 1040 °C for 2, 4, and 8 h. The hardness decreases from 4000 MPa after 2 h to ~ 3400 MPa after 8 h.

Alloy normalized at 1040 °C for 2 h was tempered at 690, 725, 745, and 790 °C for 2, 8, and 20 h. Hardness of the alloy decreased with increasing tempering temperature and time. Alloy tempered at 690 and 725 °C showed significant drop in hardness with increasing tempering time, but for 745 and 790 °C the decrease in hardness was gradual. Similar profiles were observed for samples normalized at 1040 °C for 4 h then tempered, and samples normalized at 1040 °C for 8 h then tempered at aforementioned temperatures. Among all samples normalized at 1040 °C and tempered, samples normalized for 2 h and tempered at 690 °C for 2 h had the highest hardness, while sample normalized for 8 h and tempered at 790 °C for 20 h had the lowest hardness. The tempering temperature of the sample normalized at

1040 °C for 2 h was expanded to temperatures slightly above A_{C1} temperatures. Hardness of the alloy normalized at 1040 °C for 2 h and tempered for 2 h decreased with increasing tempering temperature up to 745 °C, stabilized till 820 °C.

The $\sigma_{0.2}$, σ_B, and δ at room temperature, 600 and 650 °C for P92 steel in different heat treated conditions are determined in [94]. Except for the specimen given the usual austenization treatment (2 h at 1070 °C) but a low temperature tempering treatment (2 h at 715 °C), the yield and tensile strengths for different HTs were similar at each of the test temperatures. The low temperature tempering led to an increase in strength, especially at room temperature; this is attributed to the somewhat higher dislocation density. It should be noted that the minimum yield stress and tensile strength measured at room temperature (440 and 750 MPa, respectively) specified for P92 were met by all the HTs applied.

The high values of yield and tensile strengths are reached after partial tempering at 500 °C (500PT): 1370 and 1506 MPa, respectively [95]. After mentioned treatment the microstructure of T91 steel is dual and consists of 15% of bainitic ferrite (α_B) and 85% of partial tempered martensite ($\alpha`_{PT}$). Also, the 500PT specimen has the highest number of ε and θ carbides density ~ $2.32 \cdot 10^{13}$ m^{-2}. The best uniform elongation (8.2%) was established in AR condition. In fact, the strengthening mechanisms in the PT T91 are mainly attributed to precipitation hardening from transition carbides, solid solution strengthening from solute carbon atoms, and subgrain boundary strengthening from martensitic lath and ultra-fine martensite. The large uniform elongation arises from bainitic ferrite induced by a reduced cooling rate.

The martensitic lath width and dislocations were the main microstructural factors influencing the tensile strength of 15Cr12MoVWN steel [96]. The strengthening contribution from $M_{23}C_6$ and MX was higher than that from grain boundaries of PAG and was the other important factor for strengthening. The average sizes of PAG and $M_{23}C_6$ particles were the main factors influencing the tensile ductility. Tempering temperature had the most significant influence on the evolution of precipitates and dislocation densities. Normalizing temperature had the most significant influence on the coarsening of PAG and $M_{23}C_6$. Cooling methods had less influence in both microstructure and tensile properties compared with the other two HT parameters. Also, based on the tensile strength and elongation at 23 and 550 °C, the optimized HT parameter was determined: normalizing at 1050 °C, AC to room temperature and tempering at 700 °C. The tensile properties of specimens in optimized HT condition were 1014 MPa (σ_B), 810 MPa ($\sigma_{0.2}$), and 18.8% (elongation) tested at 23 °C, and the values were 577.5 MPa (σ_B), 469 MPa ($\sigma_{0.2}$), and 39.8% (elongation) tested at 550 °C.

The mechanical properties of HT9 steel specimens heat treated to twenty-five combinations consisting of five values of austenitization temperature Tγ (950…1200 °C) and five tempering parameters P_T ($18.5 < P_T < 21$) were investigated in [97]. Hardness and strength parameters showed a slight maximum (35 HRC and 1250 MPa, respectively) and dynamic (lower shelf) toughness a slight minimum at Tγ = 1050 °C, but in general these properties were relatively insensitive to Tγ. This is despite large changes in the PAG size and lath packet size with increasing Tγ. With increasing P_T the hardness and yield strength decreased, and the dynamic (lower shelf) toughness increased slightly. The observed variation in yield strength is most likely the result of primary dependence on dislocation density, matrix carbide dispersion and interstitial solute (carbon) content; these parameters are little affected by Tγ, but are reduced with increasing P_T.

Fig. 8 shows the hardness change of HT9 with the HT conditions obtained in [98]. The hardness was shown to increase with increase in normalizing temperature. A tensile test was carried out at room temperature and high temperature (650 ℃) to evaluate the tensile properties of the heat treated specimen under the same conditions. The tensile test was carried out at room temperature and high temperature. The yield stress shows a tendency to decrease proportionally. Yield stress was shown to increase with an increase in normalizing temperature. These tendencies were also represented at high temperature.

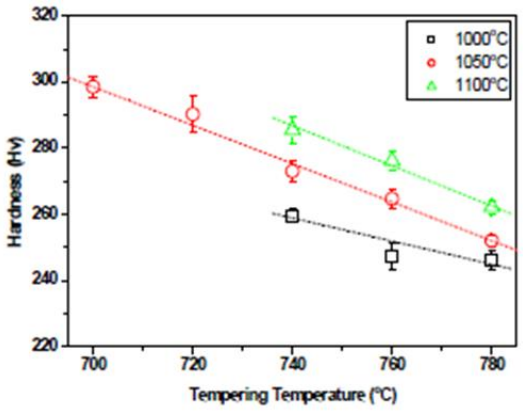

Fig. 8. Hardness change of HT9 with HT condition [98]

For T92 and Eurofer 97 steels, hardness increases with the increase of normalizing temperature [99]. From Fig. 6, we know that the grain size of T92 and Eurofer 97 increase with the increase of normalizing temperature. According to the Hall-Petch relationship, the hardness should decrease with the increase of grain size. Therefore, this indicates that there is another contribution to the hardness in T92 and Eurofer 97. The hardness of Eurofer ODS steels decreases with increased normalizing temperature. ODS FZK steel shows lower hardness than ODS HXX, possibly due to its very low carbon concentration. For T92, hardness decreases with increasing of tempering temperature. For Eurofer ODS steels, the hardness decreases with increase of tempering temperature from 550 to 750 °C, then increases at 850 °C. This suggests that some reversion to martensite takes place above 750 °C in Eurofer ODS. The HXX steel shows higher hardness than FZK. With the increase of normalizing temperature, the grain size increases in T92 and Eurofer 97 steels and remains almost unchanged in Eurofer ODS steels, the hardness increases in T92 and Eurofer 97 and decreases in Eurofer ODS steels. The formation of Nb- and Ta-rich carbides is related to the increase of hardness. Ta enrichment in yittria particles is

observed, which may be the reason for the lack of Ta-rich carbides and resulting reduction in hardness with normalizing temperature in Eurofer ODS steels. With the increase of tempering temperature, the hardness decreases in T92 while in Eurofer ODS steels, the hardness decreases until tempering temperature up to 750 °C, then increases slightly.

Higher hardness results are shown following higher temperature re-heating at 1175 °C (HV10 = 2840…3060 MPa) [100]. This is achievable following a hardenability improvement after austenite grain size growth. A strong effect of reheating temperature on austenite grain growth is detected. Tensile tests have been performed on at T = 20, 550, and 650 °C. It was established that $\sigma_{0.2}$ and σ_B after re-heating at 1175 °C + rolling at 650 °C + tempering at 720 °C are higher than that after re-heating at 1075 °C + rolling at 750 °C + tempering at 720 °C in the case of testing at room temperature and 650 °C, but vice versa at testing temperature 550 °C. Furthermore, at all 3 testing temperatures the elongation is better after reheating at 1075 °C. It seems that such behaviour is connected with a big difference in structures of specimens (see Fig. 7).

The tensile tests of the materials showed only minor variations between the different materials [101]. While the material treated at 900 °C it shows lower strength at room temperature, in the range of the operation window (550…700 °C) within the error range, no differences can be observed. The TMT brought a general increase in strength to the materials. The yield strength is approximately 50 MPa higher than the AR condition throughout the whole tested temperature range Elongations of the TMT alloys are orders of magnitude lower (0.5…2% vs. 10%) than in the initial state under the same creep conditions. Since none of the specimens have failed so far, creep-to-rupture times are expected to be greatly prolonged.

ECAP processing enhances both yield strength and ultimate tensile stress up to temperatures around 773 K [102]. Above this temperature, which is near the processing temperature, the material processed four times via route C or eight times via B_A became softer than the tempered material and the materials processed by 1 pass, or 2 passes via route C. The effect of ECAP on the temperature dependence of the hardening ratio (UTS/yield strength) is studied. In contrast to the expected result for steels, and other metals, processed by SPD, which do not exhibit significant work hardening during tensile testing, Eurofer processed by ECAP does. The hardening ratio for ECAP processed Eurofer was somewhat enhanced compared with the initial Eurofer in the investigated temperature range, except for the materials ECAP processed by 8 passes via route B_A that had a lower hardening ratio at room temperature. It is should be noted that the steep increase in the hardening ratio for the materials processed by 4 or 8 passes is accompanied by an abrupt change in the temperature trend of their uniform and fracture elongations. However, tensile behavior of materials processed by 1 pass, or 2 passes via route C, is very similar to that for the AR material.

Effect of the preliminary HT and ECAP on mechanical properties of T91 steel is described in [103]. In general, the WQ T91 steels show a combination of high strength and ductility. The yield strength of 800WQ material is 970 MPa, ~ 150 MPa lower than those heat treated above 900 °C. The uniform elongation is ~ 7% for all of the WQ T91 steel, which is insensitive to austenitizing temperature prior to WQ.

The hardness of AA specimen changes slightly and remains at ~ 2 GPa, while for 2B300 (2 passes ECAE at 300 °C) and 1000ECAE (one pass ECAE at 1000 °C and followed by WQ) the hardness value almost constant at annealing temperatures of 500 °C, but as the temperature increases, it begins to decrease sharply. Also it is worth mentioning that the softening in the 1000ECAE and 2B300 specimens after annealing may have different underlying mechanisms. As the 1000ECAE specimens have primarily martensite, its softening after tempering is due to the decomposition of martensite. In contrast, the 2B300 specimen has mostly ferrite, and the softening after annealing is primarily due to grain coarsening.

The AA specimen has a high work hardening rate and large uniform elongation as the large grains can accommodate a rapid increase of the density of mobile dislocations during deformation. In contrast, the 1000WQ specimen has less work hardening capability and uniform strain as its smaller martensite laths already contain a high density of dislocations.

The yield strength-uniform elongation paradox in T91 steels was examined [103]. Amajority of metallic materials, such as those processed by cold working, follow the general syndrome: the strengthening of a material is often accompanied by a reduction in its ductility.

As shown in Fig. 9, the TMT processes enable to tailor the mechanical properties of T91 steel over a broad range. Three distinct groups are highlighted on this plot. First, the light blue band outlines T91 steel with primarily ferrite phases. These steels were processed via ECAE at low-to-intermediate temperatures (room temperature to 700 °C). The higher strength of ferritic T91 steels originates mostly from grain refinement. The highest strength achieved in ferritic T91 steel in [103] is 1000 MPa with a mere 2% uniform elongation. In the second category (dominated by martensite shown as red band in Fig. 9), TMTs via austenitizing at 900 °C or greater (followed by WQ) and ECAE at 1000 °C induce primarily martensite. The yield strength of 1000WQ/500 10h/1A300 T91 exceeds 1600 MPa with, however, only ~ 1.5% uniform elongation. HT of the ECAE specimens leads to an improvement of uniform elongation, to ~ 4%, with a yield strength of 1400 MPa. The third category includes T91 steels processed by WQ at 800 °C or WQ at 900…1200 °C followed by a 600 °C tempering procedure as shown in the purple band. T91 processed by this route is composed of both ferrite and martensite. The formation of ferrite reduces the yield strength by ~ 150 MPa. It is noteworthy that when the austenitizing process is performed above 900 °C, WQ leads to the production of FM T91 steel composed primarily of martensite. The as-quenched martensite results in high yield strength, ~ 1200 MPa, as well as a reasonable uniform elongation, ~ 6…8% as shown by the yellow triangles. The retention of good ductility may be related to the low C concentration in T91 steel as well as auto-

tempering of martensite during the cooling process. The accomplishment of high strength with good ductility via such a simple WQ process is a very encouraging observation. While the strength and ductility of martensitic T91 (red band) and ferritic T91 (light blue band) may still follow the paradoxical relationship, ductile martensite can bring the coordinates of the strength and ductility to a greater level beyond the ferrites. The FM T91 (in the purple band) bridges the mechanical behavior between the two distinct groups (red and light blue band). This TMT roadmap thus permits the tailoring of T91 steels with various combinations of strength and ductility for different industrial and nuclear applications.

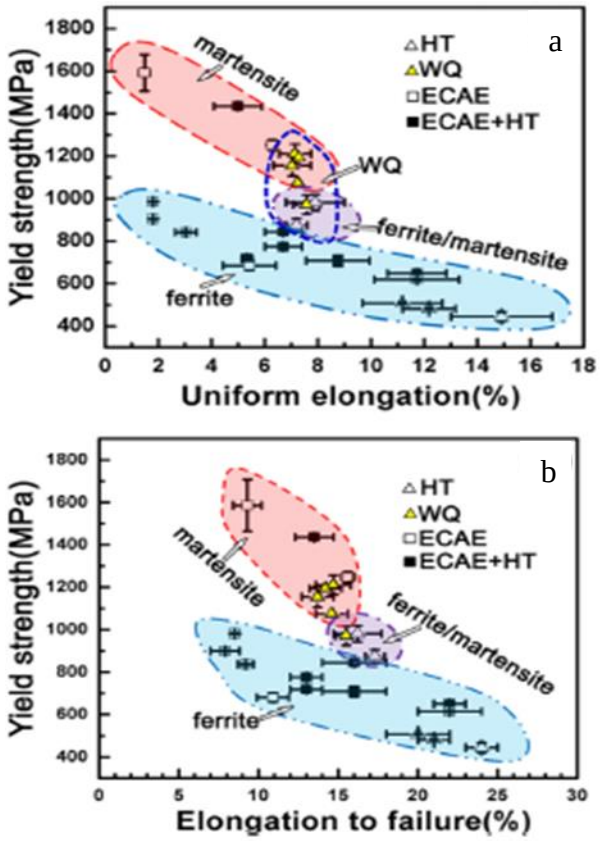

Fig. 9. Summary of yield strength-uniform elongation (a) and yield strength-elongation to failure (b) maps for T91 steel subjected to various types of TMTs [103]

The hardness of G91 steel at various HT and hot rolled conditions is investigated in [104]. The initial steel exhibits the hardness about 2770 MPa. With the reduction in tempering temperature (650 ºC), the hardness increases to ~ 3710 MPa while keeping the normalizing temperature (1050 ºC) same AR condition. At high tempering temperature, dissolved solute elements are re-precipitated in the form of $M_{23}C_6$ and MX, which results into a loss in solid solution strengthening. The loss in solid solution strengthening indicates the decrease in hardness value. In addition, hardness value increases with the increase in normalizing temperature while keeping tempering temperature same. As majority of precipitates dissolve at high normalizing tempering temperature and leads to solid solution strengthening. Previous studies show that the hardness mainly depends on primary/secondary phases of MX particles, presence of N and C in the solution, dislocation density and grain size [124]. Hardness of 9Cr-1Mo steel is less affected by prior austenite grain size rather than packet size [130]. Specimen treated at R550-T650 and R1050-T650 conditions have hardness value equal to 3680 and 3580 MPa, respectively. This might be due to high residual stress generated during hot rolling treatment.

For tempering temperatures (650 and 700 ºC), $\sigma_{0.2}$ and UTS is found to increase with the increase in normalizing temperature. Specifically, a significant increase in $\sigma_{0.2}$ and UTS is observed at tempering temperature of 650 ºC, whereas there is a reduction in $\sigma_{0.2}$ and UTS for tempering at 700 °C as compared to tempering at 650 °C. In case of N1050-T650 (N – normalization), the yield strength increases by 37.3% at 20 ºC and 73.2% at 650 ºC as compared to AR condition i.e. N1050-T750. Correspondingly, the UTS increases by 34.2% at 20 ºC and 71.5% at 650 ºC and the elongation reduces by 10.9% at 20 ºC and by 22.7% at 650 ºC. The improvement in mechanical strength at low tempering temperature (i.e. 650 ºC) suggests the contribution of precipitate size and dislocation density. The high tempering temperature (i.e. 750 ºC) causes the growth of $M_{23}C_6$ particles, subgrain boundary formation and recovery.

Specimen processed at R550-T650 and R1050-T650 has got a significant improvement in $\sigma_{0.2}$ and UTS at 650 ºC as compared to AR condition. In case of R550-T650, the $\sigma_{0.2}$ increases by 36.1% at 20 ºC and 98.0% at 650 ºC as compared to AR condition whereas the UTS increases by 54.9% at 20 ºC and 107.0% at 650 ºC. However, the elongation decreases by 32.9% at 20 °C and 37.5% at 650 ºC. The enhancement in mechanical properties followed by rolling is more as compared to heat-treated conditions. This may be due to high extent of decrease in lath width, highly dense second phase precipitates and increase in dislocation density.

For specimen treated at R1050-T650 conditions, the yield strength increases by 29.3% at 20 ºC and 76.3% at 650 ºC as compared to AR condition. Correspondingly, the UTS increases by 35.6% at 20 ºC and 74.2% at 650 ºC, and the elongation decreases by 27.7% at 20 ºC and 29.2% at 650 ºC.

The evolutions of microhardness of T91 steel with number of extrusion passes (from 1 to 6) before and after the annealing are presented in [105]. It is noted that the microhardness exhibits a relatively steep increases from initial 2700 to 3300 MPa after one pass, then gradually increases up to about 3800 MPa until six passes, implying that the grain refinement is most appreciable at the first pass, which is consistent with other researches of ECAP processing for different materials [126, 131, 132]. After the 2 h annealing at 500 °C, the microhardness drops slightly, which may result from the slight grain growth and vanishment of a number of dislocations.

The initial T91 steel exhibits an elongation of 23% and tensile strength of 730 MPa, which is higher than the elongation of 16% but is lower than the tensile strength of 848 MPa of T91 steel in Ref. [133]. After single and 6 extrusion passes, the tensile strength increases to 920 and 1160 MPa while the elongation drastically drops to 16 and 10%, respectively. With the increasing number of

extrusion passes the tensile strength increases while the elongation decreases. This suggests that the improvement in strength accompanies with the loss of the ductility in the ECAPed T91 steel. After the annealing at 500 °C for 2 h, the tensile strength of the samples extruded one and six passes decreases to 880 and 1140 MPa, while the elongation increases to 21 and 12%, respectively. Similarly, an evident drop in tensile strength had been observed when annealing temperatures were elevated to 600 and 700 °C [134]. In general, the ductility of the ECAPed samples can be improved by annealing at the expense of a little decrease of tensile strength. However, the slight increase of tensile strength after annealing for the two passes and four passes ECAPed samples is abnormal, which may be attributed to the experimental errors caused by the small sample dimension (16 × 1.7 × 1 mm) and the estimation of the tensile strength.

The effect of UE number and subsequent HT of T91 steel on mechanical properties is studied in [106]. From Fig. 10,a it can be seen that with a grain size decreasing (consequently, with an increase in the number of UE cycles) the hardness of the samples increases and reaches the value of ~ 2900 MPa after 5 cycles of UE (vs. ~ 1900 MPa without deformation). It was established that optimal temperature of HT is 550 °C at which a high level of hardness is maintained up to 100 h of exposure. What is more for thermal treatment at this temperature during 25 h low increase in microhardness is observed (approximately by 100 MPa) despite the increase in grain size from 145 to 245 nm, decrease in dislocation density from $5.4 \cdot 10^{10}$ to $2.88 \cdot 10^{10}$ cm^{-2} and decrease in concentration of carbon dissolved into matrix from 0.053 to 0.0124 wt.%. The reason for this is, apparently, the formation of high number of fine MX-type precipitates during thermal treatment, which induce the increase in dispersion hardening. At T = 600 °C and higher the intensive growth of grains occurs also as abrupt decrease in microhardness with the increase in time of thermal treatment (see Fig. 10,b). The effect of dispersion hardening occurs to be insufficient for compensation of strength loss induced by the grain size increase.

Strength characteristics of steel T91 ($\sigma_{0.2}$ and σ_B) with submicron ferritic microstructure, obtained by SPD and by SPD with subsequent thermal treatment exceed characteristics of steel with martensitic microstructure obtained by standard processing "normalization + tempering" in temperature range -196…+550 °C. Herewith their ductility remains on sufficient level. It was revealed for the first time that in specimens of steel T91 with martensitic microstructure with a decrease of testing temperature in range of liquid nitrogen not only strength increases but also ductility improves (rupture elongation δ). For specimens with ferritic microstructure such behavior was not observed. This difference is probably related to the structural features of the martensitic laths boundaries. But further investigation is necessary to explain this effect.

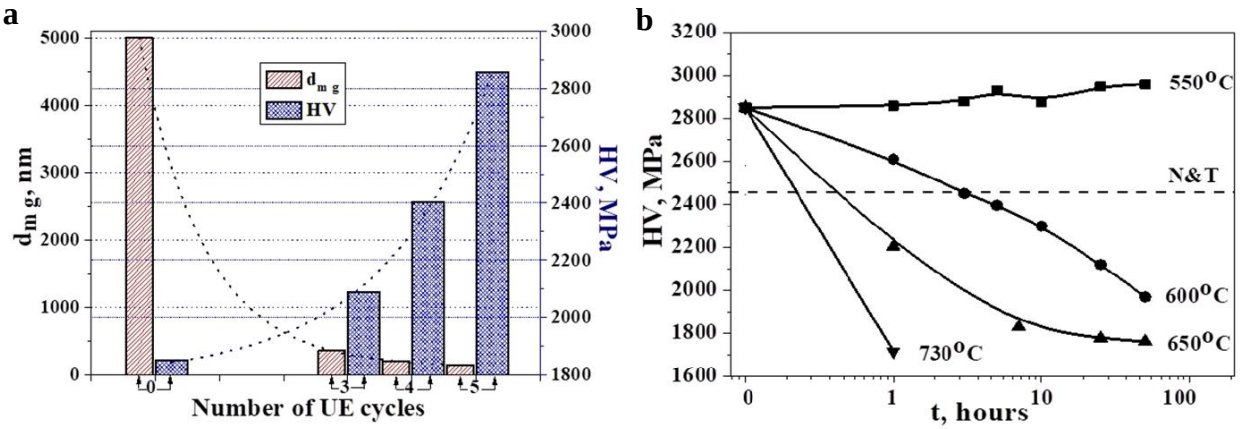

Fig. 10. Dependence of the mean grain size (d_{mg}) and microhardness (HV) of T91 steel with the number of cycles (zero cycle corresponds to the specimen exposed at 750 °C during 15 min) (a); dependence of microhardness of specimens subjected to 5 cycles of upsetting-extrusion on time of HT at different temperatures (b). Dashed line defines the level of microhardness in initial state (tempered martensite) [106]

Finally, the characteristics of strength (σ_0, the proportionality limit; σ_B, the ultimate tensile strength) and plasticity (δ, the rupture elongation) of 12CrWMoNbVB after upsetting and the next HT was studied in [108].

The strength properties of materials decrease monotonically as the test temperature rises. The highest values of hardness are obtained after upsetting (~ 3700 MPa), the lowest – after upsetting and tempering at 720 °C for hour (~ 2800 MPa), the hardness of initial sample was ~ 2620 MPa.

Upsetting led to an increase in steel strength characteristics relative to their values for initial state in the range from ~ 10 to ~ 60%, depending on the test temperature. Tempering after ausforming led to a drop in the values of σ_0 and σ_B in the entire temperature range of research, but nevertheless these characteristics remained predominantly higher than in initial sample. The relative elongation of the sample of 12CrWMoNbVB steel after ausforming decreases relative to the values in standard steel. Tempering increases the δ values, and at high test temperatures (550 and 650 °C) they exceed those in the standard steel (~ 10 %).

CONCLUSIONS

This review considers the main traditional and reduced activation 9…12% Cr FM steels chosen as structural materials for future generation reactors due to their excellent radiation tolerance, acceptable mechanical characteristics, high thermal conductivity and low thermal expansion in comparison with conventional austenitic steels. The effect of TMT and HT on the structure and mechanical properties of these steels has been studied. Based on the above, the following conclusions can be drawn:

1. Normalization temperature affects grain size, while cooling rate and tempering temperature have little effect on grain growth. At the same time, with an increase in the normalization temperature, despite grain growth, the hardness of 9…12% Cr steels in most cases also increases. This is mainly related to the formation of Nb- and Ta-rich carbides, that is precipitation strengthening.

2. It was defined, that the mass fraction of $M_{23}C_6$ precipitates remained constant up to the A_{C1} temperature but decreased drastically as austenite phase started forming. Given that austenite has higher affinity for C than α-ferrite, the $M_{23}C_6$ precipitates exist up to 865 °C, and then dissolve into the austenitic matrix. The mass fraction of MX type precipitates is constant till A_{C3} temperature, but then gradually decreased with increased temperature and totally dissolved at ~ 1200 °C.

3. Various types of thermal (normalizing, austenitizing, partial tempering, water and oil quenching) and thermomechanical (ausforming, equal channel angular pressing or extrusion, rolling, multiple "upsetting-extrusion", upsetting) treatment of 9…12% Cr steels are presented. It was found that 9% Cr FM steels became better subjected to TMT, and 12% Cr – to HT. But for 9% Cr FM steels, HT is also provided to improve structural factors with the following TMT procession.

4. Atypical thermal and thermomechanical treatments of 9% Cr FM steels are considered. It has been established that preliminary HT by the partial tempering method makes it possible to modernize the structure before subsequent mechanical treatment. MUE allows to achieve an ultrafine grained structure and qualitatively improve the characteristics of T91 steel.

5. It is necessary to carry out comprehensive studies of the effect of phases formed in FM steels after water quenching on high-temperature characteristics and radiation resistance.

ACKNOWLEDGEMENTS

The work was financially supported by the National Academy of Science of Ukraine (program "Support of the development of main lines of scientific investigations" (KPKVK 6541230)).

REFERENCES

1. L.K. Mansur et al. Materials needs for fusion, Generation IV fission reactors and spallation neutron sources – similarities and differences // *J. Nucl. Mater*. 2004, v. 329-333, p. 166-172.

2. S.M. Goldberg, R. Rosner. *Nuclear reactors: generation to generation*. Cambridge, MA: American Academy of Arts and Sciences, 2011, 29 p.

3. R. Klueh, D. Harries. *High-Chromium Ferritic and Martensitic Steels for Nuclear Applications*. West Conshohocken: ASTM International, 2001, 221 p.

4. R.L. Klueh, A.T. Nelson. Ferritic/martensitic steels for next-generation reactors // *J. Nucl. Mater*. 2007, v. 371, issue 1-3, p. 37-52.

5. C. Cabet, F. Dalle, E. Gaganidze, J. Henry, H. Tanigawa. Ferritic-martensitic steels for fission and fusion applications // *J. Nucl. Mater.* 2019, v. 523, p. 510-537.

6. T. Jayakumar, M.D. Mathew, K. Laha. High temperature materials for nuclear fast fission and fusion reactors and advanced fossil power plants // *Procedia Eng*. 2013, v. 55, p. 259-270.

7. J.S. Cheon et al. Sodium fast reactor evaluation: Core materials // *J. Nucl. Mater*. 2009, v. 392, issue 2, p. 324-330.

8. C. Cawthorne, E. Fulton. Voids in irradiated stainless steel // *Nature*. 1967, v. 216, p. 575-576.

9. F. Masuyama. New developments in steels for power generation boilers // *Advanced Heat Resistant Steels for Power Generation.* London: IOM Communications Ltd, 1999, p. 33.

10. J.W. Davis, D.J. Michel. *Topical Conference on Ferritic Alloys for Use in Nuclear Energy Technologies*. Warrendale, PA: The Metallurgical Society of AIME, 1984, p. 261.

11. J. Bishop. Metallurgy in relation to reactor design and development // *Dimensional stability and mechanical behavior of irradiated metals and alloys.* London: Thomas Telford Publishing, 1984, p. 115.

12. J.W. Bennett, K.E. Horton. Materials requirements for liquid metal fast breeder reactors // *Metall. Mater. Trans. A*. 1978, v. 9, issue 2, p. 143-149.

13. H. Brager, J. Perrin. *Effects of Radiation on Materials: Eleventh Conference*. Philadelphia PA: American Society for Testing and Materials, 1982, p. 1197.

14. R.L. Klueh, J.P. Shingledecker, R.W. Swindeman, D.T. Hoelzer. Oxide dispersion-strengthened steels: A comparison of some commercial and experimental alloys // *J. Nucl. Mater.* 2005, v. 341, issue 2-3, p. 103-114.

15. R.L. Klueh. Elevated temperature ferritic and martensitic steels and their application to future nuclear reactors // *Int. Mater. Rev*. 2005, v. 50, issue 5, p. 287-310.

16. S.J. Zinkle, J.T. Busby. Structural materials for fission and fusion energy // *Mater. Today*. 2009, v. 12, issue 11, p. 12-19.

17. C. Fazio et al. European cross-cutting research on structural materials for Generation IV and transmutation systems // *J. Nucl. Mater.* 2009, v. 392, issue 2, p. 316-323.

18. L. Malerba et al. Materials for Sustainable Nuclear Energy: A European Strategic Research and Innovation Agenda for All Reactor Generations // *Energies*. 2022, v. 15, issue 5, p. 1845.

19. E.A. Little, D.A. Stow. Void-swelling in irons and ferritic steels: II. An experimental survey of materials irradiated in a fast reactor // *J. Nucl. Mater.* 1979, v. 87, issue 1, p. 25-39.

20. V.N. Voyevodin, G.D. Tolstolutskaya, M.A. Tikhonovsky, A.S. Kuprin, A.S. Kalchenko. Mechanisms of radiation damage and development of structural materials for operating and advanced nuclear reactors // *Problems of Atomic Science and Technology (PAST)*. 2021, N 5(135), p. 3-20.

21. E. Getto et al. Void swelling and microstructure evolution at very high damage level in self-ion irradiated ferritic-martensitic steels // *J. Nucl. Mater*. 2016, v. 480, p. 159-176.

22. V. Voyevodin et al. Structural features and operational characteristics of steel T91 // *East Eur. J. Phys*. 2020, v. 3, p. 93-98.

23. S. Nomura et al. Development of long life FBR core materials // *Proceedings of the International Conference on Fast Reactors and Related Fuel Cycles*. Tokyo: Atomic Energy Society of Japan, 1991, Paper 7.4.

24. A. Uehira, S. Ukai, T. Mizuno, T. Asaga, E. Yoshida. Tensile Properties of llCr-0.5Mo-2W, V, Nb Stainless Steel in LMFBR Environment // *J. Nucl. Sci. Technol*. 2000, v. 37, p. 780-786.

25. K. Anderko. Zur eignung warmfester vergütungsstähle mit 9 bis 12% chrom für komponenten im kern schneller reaktoren – ein überblick // *J. Nucl. Mater.* 1980, v. 95, p. 31-43.

26. Technical reports. *Structural materials for liquid metal cooled fast reactor fuel assemblies operational behaviour*. Vienna: International Atomic Energy Agency, 2012, p. 19.

27. C. Brown et al. Cladding and wrapper development for fast breeder reactor high performance // *Proceedings of the International Conference on Fast Reactors and Related Fuel Cycles.* Tokyo: Atomic Energy Society of Japan, 1991, Paper 7.5.

28. J.W. Davis, D.J. Michel. *Topical Conference on Ferritic Alloys for Use in Nuclear Energy Technologies*. Warrendale, PA: The Metallurgical Society of AIME, 1984, p. 299.

29. A. Lovell, A. Fox, W. Sutherland, S. Hecht. Demonstration of a high burnup heterogeneous core using ferritic/martensitic materials // *Proceedings of the International Conference on Reliable Fuels for Liquid Metal Reactors*. Richland, WA: American Nuclear Society, 1987, p. 3.

30. R. Viswanathan. Materials technology for coal fired power plants // *Adv. Mater. Process*. 2004, v. 162, p. 73-76.

31. B.H. Sencer, J.R. Kennedy, J.I. Cole, S.A. Maloy, F.A. Garner. Microstructural analysis of an HT9 fuel assembly duct irradiated in FFTF to 155 dpa at 443° C // *J. Nucl. Mater*. 2009, v. 393, p. 235-241.

32. P. Gavoille et al. Mechanical Properties of Cladding and Wrapper Materials for the ASTRID Fast-Reactor Project // *Proceedings of the International Conference on Fast Reactors and Related Fuel Cycles: Safe Technologies and Sustainable Scenarios.* Vienna: International Atomic Energy Agency, 2013, Paper T4.2.

33. C. Fazio, P. Dubuisson. Achievement and new challenges for high performance materials in Europe // *Proceedings of the International Conference on Fast Reactors and Related Fuel Cycles: Safe Technologies and Sustainable Scenarios.* Vienna: International Atomic Energy Agency, 2013, p. 487.

34. T. Asayama et al. Development of structural materials for JSFR – overview and current status // *International Conference on Fast Reactors and Related Fuel Cycles.* Vienna: International Atomic Energy Agency, 2009, p. 417-431.

35. D. Zhang // *49th Meeting of the Technical Working Group on Fast Reactors (TWG-FR),* Buenos Aires, Argentina, 2016.

36. J. Yoo. Korean SFR development program and technical activity for improving economical competitiveness // *Technical Meeting on Fast Reactors and Related Fuel Cycle Facilities with Improved Characteristics, IAEA.* Vienna, Austria, 2013.

37. T. Ma, X. Hao, P. Wang. Effect of heat treatments on Charpy impact properties of 15Cr12MoVWN ferritic/martensitic steel // *J. Iron Steel Res. Int.* 2022, v. 29, p. 512-518.

38. R.L. Klueh, D.J. Alexander. Heat treatment effects on impact toughness of 9Cr-1MoVNb and 12Cr-1MoVW steels irradiated to 100 dpa // *J. Nucl. Mater.* 1998, v. 253-258, p. 1269-1274.

39. D. S. Gelles. Development of martensitic steels for high neutron damage applications // *J. Nucl. Mater.* 1996, v. 239, p. 99-106.

40. N.M. Ghoniem, J. Blink, N. Hoffman. Selection of alloy steel type for fusion power plant applications in the 350-500 °C range // *Proc. of the Topical Conf. on Ferritic Alloys for Use in Nuclear Technology,* Snowbird, Utah, 1983.

41. D. Gilbon, C. Rivera. Behavior of different ferritic steels under ion, electron and fast neutron irradiation // *J. Nucl. Mater.* 1988, v. 155-157, p. 1268-1273.

42. T.R. Allen, J.T. Busby, R.L. Klueh, S.A. Maloy, M.B. Toloczko. Cladding and duct materials for advanced nuclear recycle reactors // *JOM*. 2008, v. 60, N 1, p. 15-23.

43. D. Frazer et al. Degradation of HT9 under simultaneous ion beam irradiation and liquid metal corrosion // *J. Nucl. Mater*. 2016, v. 479, p. 382-389.

44. Y. Kurata, M. Futakawa, S. Saito. Comparison of the corrosion behavior of austenitic and ferritic/martensitic steels exposed to static liquid Pb-Bi at 450 and 500 °C // *J. Nucl. Mater*. 2005, v. 343, p. 333-340.

45. R. Lindau et al. Present development status of EUROFER and ODS-EUROFER for application in blanket concepts // *Fus. Eng. Des.* 2005, v.75-79, p. 989-996.

46. D. Kumar et al. The effects of fusion reactor thermal transients on the microstructure of Eurofer-97 steel // *J. Nucl. Mater*. 2021, v. 554, p. 153084.

47. G. Mazzone et al. Choice of a low operating temperature for the DEMO EUROFER97 divertor cassette // *Fusion Eng. Des*. 2017, v. 124, p. 655-658.

48. J. Roth et al. EUROFER as wall material: Reduced sputtering yields due to W surface enrichment // *J. Nucl. Mater.* 2014, v. 454, p. 1-6.

49. J.H. You et al. Divertor of the European DEMO: Engineering and technologies for power exhaust // *Fusion Eng. Des*. 2022, v. 175, p. 113010.

50. G. Benamati et al. Mechanical and corrosion behaviour of EUROFER 97 steel exposed to Pb-17Li // *J. Nucl. Mater*. 2002, v. 307-311, p. 1391-1395.

51. V. Sikka, C. Ward, K. Thomas. Modified 9Cr-1Mo steel – an improved alloy for steam generator applications // *Proc. International Conf. on Ferritic Steels for High Temperature Applications.* Metals Park, OH: American Society for Metals, 1983, p. 65.

52. G. Bodine, R. McDonald. Laboratory and pilot commercial process/product development of modified 9Cr-1Mo ferritic alloy // *Proc. International Conf. on Ferritic Steels for High Temperature Applications*. Metals Park, OH: American Society for Metals, 1983, p. 9-20.

53. G. Cunningham, P. Patriarca, E. Hoffman. Ferritic steels as alternate structural materials for high-temperature applications // *Proc. International Conf. on Ferritic Steels for High Temperature Applications*. Metals Park, OH: American Society for Metals, 1983, p. 3-6.

54. B. Roberts, R. Swindeman. TVA experience in the application of 9Cr-1Mo-0.2V-CB (Grade 91) steel // *Proceedings of the EPRI Conference on 9Cr Materials Fabrication and Joining Technologies*. Charlotte, NC: Fossil Repair Applications Center (FRAC), 2001, Paper 20-1.

55. R. Swindeman, M. Santella, P. Maziasz, B. Roberts, K. Coleman. Issues in replacing Cr-Mo steels and stainless steels with 9Cr-1Mo-V steel // *Int. J. Press. Vessel. Pip*. 2004, v. 81, p. 507-512.

56. S. Dubiez-Legoff et al. Selection of materials for sodium fast reactor steam generators // *Proceedings of the 2012 International Congress on Advances in Nuclear Power Plants – ICAPP '12.* La Grange Park, IL: American Nuclear Society, 2012, Paper 12053.

57. C. Cabet, F. Rouillard. Corrosion phenomena induced by gases in Generation IV nuclear reactors // *Structural materials for generation IV nuclear reactors*. Sawston: Woodhead Publishing, 2017, p. 75-104.

58. S.C. Chetal et al. Current Status of Fast Reactors and Future Plans in India // *Energy Procedia*. 2011, v. 7, p. 64-73.

59. K. Aoto et al. Design study and R&D progress on Japan sodium-cooled fast reactor // *J. Nucl. Sci. Technol*. 2011, v. 48, p. 463-471.

60. Y. Chikazawa et al. Evaluation of JSFR key technologies // *Nucl. Technol*. 2012, v. 179, p. 360-373.

61. https://www.westinghousenuclear.com/new-plants/lead-cooled-fast-reactor

62. G. Bauer, M. Salvatores, G. Heusener. MEGAPIE, a 1 MW pilot experiment for a liquid metal spallation target // *J. Nucl. Mater*. 2001, v. 296, p. 17-33.

63. F. Bianchi et al. Status and trend of core design activities for heavy metal cooled accelerator driven system // *Energy Convers. Manag*. 2006, v. 47, p. 2698-2709.

64. Y. Dai et al. Assessment of the lifetime of the beam window of MEGAPIE target liquid metal container // *J. Nucl. Mater*. 2006, v. 356, p. 308-320.

65. W. Wagner, F. Gröschel, K. Thomsen, H. Heyck. MEGAPIE at SINQ – The first liquid metal target driven by a megawatt class proton beam // *J. Nucl. Mater*. 2008, v. 377, p. 12-16.

66. A. Alemberti et al. European lead fast reactor–ELSY // *Nucl. Eng. Des*. 2011, v. 241, p. 3470-3480.

67. A. Alemberti. European Strategy for LFRs Development // *Proceedings of the International Workshop on Innovative Nuclear Reactors Cooled by Heavy Liquid Metals: Status and Perspectives*, Pisa, Italy, 2012.

68. A. Alemberti, V. Smirnov, C. Smith, M. Takahashi. Overview of lead-cooled fast reactor activities // *Prog. Nucl. Energy*. 2014, v. 77, p. 300-307.

69. H. Abderrahim, P. Baeten, D. Bruyn, R. Fernandez. MYRRHA – A multi-purpose fast spectrum research reactor // *Energy Convers. Manag*. 2012, v. 63, p. 4-10.

70. P. Schuurmans. *Technical Meeting on Liquid Metal Reactor Concepts: Core Design and Structural Materials*, Jun 2013, Vienna (Austria).

71. W.R. Corwin et al. Generation IV reactors integrated materials technology program plan: focus on very high temperature reactor materials // *Technical Report*. United States, 2008; doi:10.2172/951084.

72. D. Hittner et al. RAPHAEL: Development of advanced technologies for high and very high temperature reactors // *Proceedings of the FISA.* Luxembourg: Office for Official Publ. of the European Communities, 2006, p. 196-209.

73. C. Poette et al. Status of the ETDR Design // *Proceedings of the ICAPP 2007 Conference*, 13-18 May 2007, Nice, France, Paper 7208.

74. H. Burlet et al. Evaluation of Nickel-Based Materials for VHTR Heat Exchanger // *Proceedings of the OECD NEA NSC Workshop on Structural Materials for Innovative Nuclear Systems (SMINS)*. London: OECD Publishing, 2008, p. 79.

75. F. Carre, P. Yvon, P. Anzieu, N. Chauvin, J.-Y. Malo. Update of the French R&D strategy on gas-cooled reactors // *Nucl. Eng. Des*. 2010, v. 240, p. 2401-2408.

76. G. Was et al. Corrosion and stress corrosion cracking in supercritical water // *J. Nucl. Mater*. 2007, v. 371, p. 176-201.

77. C. Sun, R. Hui, W. Qu, S. Yick. Progress in Corrosion Resistant Materials for Supercritical Water Reactors // *Corros. Sci*. 2009, v. 51, p. 2508-2523.

78. P. Hejzlar et al. TERRAPOWER, LLC traveling wave reactor development program overview // *Nucl. Eng. Tech.* 2013, v. 45, p. 731-744.

79. G. Was et al. Emulation of reactor irradiation damage using ion beams // *Scripta Mater*. 2014, v. 88, p. 33-36.

80. J. Wharry, G. Was. A systematic study of radiation-induced segregation in ferritic–martensitic alloys // *J. Nucl. Mater*. 2013, v. 442, p. 7-16.

81. J. Gigax et al. Radiation response of alloy T91 at damage levels up to 1000 peak dpa // *J. Nucl. Mater*. 2016, v. 482, p. 257-265.

82. E. Getto, G. Vancoevering, G. Was. The co-evolution of microstructure features in self-ion irradiated HT9 at very high damage levels // *J. Nucl. Mater*. 2017, v. 484, p. 193-208.

83. A. Alamo, V. Lambard, X. Averty, M.H. Mathon. Assessment of ODS-14%Cr ferritic alloy for high

temperature applications // *J. Nucl. Mater*. 2004, v. 329-333, p. 333-337.

84. R. L. Klueh. Analysis of swelling behaviour of ferritic/martensitic steels // *Philos. Mag*. 2008, v. 98, issue 28, p. 2618-2636.

85. M. Rieth et al. *EUROFER 97 Tensile, charpy, creep and structural tests (FZKA – 6911).* Germany, 2003.

86. https://www.astm.org/a0213_a0213m-18.html

87. H. Zhang, B. Long, Y. Dai. Metallography studies and hardness measurements on ferritic/martensitic steels irradiated in STIP // *J. Nucl. Mater*. 2008, v. 377, issue 1, p. 122-131.

88. E.B. Kula, M. Azrin. Thermomechanical Processing of Ferrous Alloys // *Advances in Deformation Processing.* Boston, MA: Springer, 1978, p. 245-300.

89. V.F. Zackay. Thermomechanical processing // *Mater. Sci. Eng*. 1976, v. 25, p. 247-261.

90. S. Yue. Thermomechanical processing of ferrous alloys // *Metalworking: Bulk Forming*: ASM Handbook. Materials Park, OH: ASM International, 2005, v. 14A, p. 286-296.

91. G.E. Totten. *Steel heat treatment: metallurgy and technologies* (*2nd ed.)*. Boca Raton, FL: CRC Press, 2007, 1576 p.

92. T. Shrestha et al. Effect of heat treatment on microstructure and hardness of Grade 91 steel // *Metals*. 2015, v. 5, p. 131-149.

93. N.Z. Gutiérrez et al. Heterogeneous austenite grain growth in ASTM A213–T91 Steel // *ISIJ Int*. 2007, v. 47, N 8, p. 1178-1187.

94. P.J. Ennis et al. Influence of heat treatments on microstructural parameters and mechanical properties of P92 steel // *Mater. Sc. and Techn.* 2000, v. 16, issue 10, p. 1226-1233.

95. Z. Shang et al. Tailoring the strength and ductility of T91 steel by partial tempering treatment // *Acta Mater*. 2019, v. 169, p. 209-224.

96. T. Ma et al. Effect of heat treatments on microstructural evolution and tensile properties of 15Cr12MoVWN ferritic/martensitic steel // *Metals*. 2020, v. 10, p. 1271.

97. R. Maiti et al. Mechanical properties of HT-9 as a function of heat treatment // *J. Nucl. Mater*. 1986, v. 141-143, p. 527-531.

98. H.M. Heo et al. Effect of heat treatment and aging conditions on the microstructure and mechanical properties of HT9 steel for fuel cladding tube // *Korean J. Met. Mater*. 2015, v. 53, № 3, p. 177-186.

99. Z. Lu et al. Effect of heat treatment on microstructure and hardness of Eurofer 97, Eurofer ODS and T92 steels // *J. Nucl. Mater*. 2009, v. 386-388, p. 445-448.

100. C. Testani et al. Austenitization and tempering temperatures effects on EUROFER 97 steel // *Materials Science Forum*. 2018, v. 941, p. 711-716.

101. J. Hoffmann et al. Improvement of reduced activation 9%Cr steels by ausforming // *Nucl. Mater. Energy*. 2016, v. 6, p. 12-17.

102. P. Fernández et al. Microstructural and mechanical characteristics of EUROFER'97 processed by equal channel angular pressing // *J. Nucl. Mater*. 2011, v. 417, p. 20-24.

103. M. Song et al. A roadmap for tailoring the strength and ductility of ferritic/martensitic T91 steel via thermo-mechanical treatment // *Acta Mater*. 2016, v. 112, p. 361-377.

104. S.S. Samant et al. Influence of intermediate rolling on mechanical behavior of modified 9Cr-1Mo steel // *Mater. Sci. Eng. A*. 2018, v. 738, p. 135-152.

105. Z.Q. Fan et al. The microstructure and mechanical properties of T91 steel processed by ECAP at room temperature // *J. Nucl. Mater*. 2013, v. 434, p. 417-421.

106. V.N. Voyevodin et al. A new approach to thermo-mechanical treatment of steel T91 by multiple upsetting-extrusion in a ferritic range // *Mater. Sci. Eng. A*. 2021, v. 822, 141686;
https://doi.org/10.1016/j.msea.2021.141686

107. Патент 42487 А Україна, МПК 7 H01B12/00. *Спосіб виготовлення ніобій-титанового надпровідник* / О.В. Чорний, Я.Д. Стародубов, О.І. Волчок, Г.Є. Сторожилов. Бюл. №9. Заявл. 12.03.2001; Опубл. 15.10.2001.

108. I.F. Kislyak et al. Effect of ausforming on mechanical properties of 12%Cr ferritic/martensitic steel // *Problems of Atomic Science and Technology*. 2022, N 1(137), p. 76-84.

109. Y.Z. Shen et al. Identification of precipitate phases in a 11Cr ferritic/martensitic steel using electron microdiffraction // *J. Nucl. Mater*. 2010, v. 400, p. 64-68.

110. P. Anderson, T. Bellgard, F.L. Jones. Creep deformation in a modified 9Cr-1Mo steel // *Mater. Sci. Technol*. 2003, v. 19, p. 207-213.

111. F. Abe, S. Nakazawa, H. Araki, T. Noda. The role of microstructural instability on creep behaviour of a low radioactivation martensitic 9Cr-2 W steel // *Metal. Trans. A*. 1992, v. 23, p. 469-477.

112. M. Tamura et al. Development of potential low activation ferritic and austenitic steels // *J. Nucl. Mater*. 1986, v. 141-143, p. 1067-1073.

113. M. Tamura, K. Ikeda, H. Esaka, K. Shinozuka. Precipitation behavior of NbC in 9%Cr1%Mo0.2%VNb steel // *ISIJ Int.* 2001, v. 41, p. 908-914.

114. R. C. Wilcox, B. A. Chin. Austenitizing and microstructure of a HT-9 steel // *Metallography*. 1984, v. 17, issue 3, p. 285-298.

115. P. Fernandez et al. Reduced Activation Ferritic/Martensitic Steel Eurofer 97 as Possible Structural Material for Fusion Devices Metallurgical Characterization on As-Received Condition and after Simulated Services Conditions // *CIEMAT-1048*, Spain, 2004.

116. H. Rostova et al. Cavitation wear of Eurofer 97, Cr18Ni10Ti and 42HNM alloys // *Acta Polytechnica*. 2021, v. 61(6), p. 762-767.

117. X. Hu, N. Xiao, X. Luo, D. Li. Effects of δ-ferrite on the microstructure and mechanical properties in a tungsten-alloyed 10 %Cr ultra-supercritical steel // *Acta Metall. Sin*. 2009, v. 45, p. 553-558.

118. P. Hu et al. Nitride-strengthened reduced activation ferritic/martensitic steels // *Fusion Eng. Des*. 2010, v. 85, p. 1632-1637.

119. J.W. Davis, D.J. Michel. *Topical Conference on Ferritic Alloys for Use in Nuclear Energy Technologies*.

Warrendale, PA: The Metallurgical Society of AIME, 1984, p. 299.

120. J.W. Davis, D.J. Michel. *Topical Conference on Ferritic Alloys for Use in Nuclear Energy Technologies*. Warrendale, PA: The Metallurgical Society of AIME, 1984, p. 347.

121. K. Anderko, L. Schäfer, E. Materna-Morris. Effect of the δ-ferrite phase on the impact properties of martensitic chromium steels // *J. Nucl. Mater*. 1991, v. 179-181, p. 492-495.

122. Г.Ю. Ростова та ін. Кавітаційне зношування ферритно-мартенситної сталі Т91 // *Фізико-хімічна механіка матеріалів (ФХММ)*. 2022, №3, с. 79-83.

123. A. Zielinska-Lipiec, A. Czyrska-Filemonowicz, P.J. Ennis, O. Wachter. The influence of heat treatments on the microstructure of 9% chromium steels containing tungsten // *J. Mater. Process. Technol*. 1997, v. 64, p. 397-405.

124. D.R. Barbadikar et al. Effect of normalizing and tempering temperatures on microstructure and mechanical properties of P92 steel // *Int. J. Pres. Ves. Pip.* 2015, v. 132, p. 97-105.

125. Z.G. Liu et al. Electron-microscopy investigation on nanocrystal formation in pure Fe and carbon steel during ball milling // *Mater. Sci. Eng. A*. 2003, v. 362, p. 322-326.

126. D.H. Shin, I. Kim, J. Kim, K.T. Park. Grain refinement mechanism during equal-channel angular pressing of a low-carbon steel // *Acta Mater*. 2001, v. 49, p. 1285-1292.

127. J.Y. Huang, Y.T. Zhu, H. Jiang, T.C. Lowe. Microstructures and dislocation configurations in nanostructured Cu processed by repetitive corrugation and straightening // *Acta Mater*. 2001, v. 49, p. 1497-1505.

128. G.J. Raab, R.Z. Valiev, T.C. Lowe, Y.T. Zhu. Continuous processing of ultrafine grained Al by ECAP-Conform // *Mater. Sci. Eng. A*. 2004, v. 382, p. 30-34.

129. J. Vivas et al. Effect of ausforming temperature on the microstructure of G91 steel // *Metals.* 2017, v. 7, p. 236.

130. A. Chatterjee, D. Chakrabarti, A. Moitra, R. Mitra, A.K. Bhaduri. Effect of deformation temperature on the ductile-brittle transition behavior of a modified 9Cr-1Mo steel // *Mater. Sci. Eng. A.* 2015, v. 630, p. 58-70.

131. B.Q. Han, S. Yue. Processing of ultrafine ferrite steels // *J. Mater. Process Technol*. 2003, v. 136, p. 100-104.

132. W.Q. Cao et al. Strain path effects on the microstructure evolution and mechanical properties of Zr702 // *Mater. Sci. Eng. A*. 2005, v. 395, p. 77-86.

133. J. Henry, X. Averty, Y. Dai, J.P. Pizzanelli. Tensile behaviour of 9Cr-1Mo tempered martensitic steels irradiated up to 20 dpa in a spallation environment // *J. Nucl. Mater*. 2008, v. 377, p. 80-93.

134. D.C. Foley, K.T. Hartwig, S.A. Maloy, P. Hosemann, X. Zhang. Grain refinement of T91 alloy by equal channel angular pressing // *J. Nucl. Mater*. 2009, v. 389, p. 221-224.

Article received 22.07.2022

ЛІТЕРАТУРНИЙ ОГЛЯД: ФЕРИТНО-МАРТЕНСИТНІ СТАЛІ – ОБРОБКА, СТРУКТУРА ТА МЕХАНІЧНІ ВЛАСТИВОСТІ

Г.Ю. Ростова, Г.Д. Толстолуцька

Вживання електроенергії, що постійно зростає, вимагає розробки та впровадження більш потужних та енергоємних систем нового покоління. Ядерні та термоядерні установки четвертого покоління (Gen-IV) дадуть можливість покрити зростаючий попит на електроенергію. Оскільки реактори Gen-IV працюватимуть за вищих температур і доз опромінення, виникає проблема підбора науково обґрунтованих конструкційних матеріалів, так як реакторні матеріали, що нині використовуються, не придатні для використання в таких жорстких умовах експлуатації. Серед конструкційних матеріалів, що розглядаються, для майбутніх поколінь реакторів особлива увага приділяється 9…12% Cr феритно-мартенситним сталям через їх більш високу радіаційну толерантність і відмінні механічні властивості порівняно з традиційно використовуваними аустенітними сталями. У даному огляді розглянуті основні феритно-мартенситні сталі, які будуть використовуватися як конструкційні матеріали, їх структура, механічні властивості та різні термічні та термомеханічні обробки, що застосовуються до них.

.